LAPPEENRANTA-LAHTI UNIVERSITY OF TECHNOLOGY LUT
LUT School of Energy Systems
Degree Programme in Energy Systems
Master's Thesis

Jordan Blake Banks

HYDROTHERMAL CARBONIZATION OF PULP MILL SLUDGE: CHARACTERIZATION AND EFFECTS OF LIQUID FRACTION RECIRCULATION

Lappeenranta, 2021

Examiners: Professor Esa Vakkilainen
D.Sc. (Tech) Ekaterina Sermyagina
Supervisors: Professor Esa Vakkilainen
D.Sc. (Tech) Clara Lisseth Mendoza Martinez

ABSTRACT

Lappeenranta-Lahti University of Technology LUT
LUT School of Energy Systems
Degree Programme in Energy Systems

Jordan Blake Banks

Hydrothermal carbonization of pulp mill sludge: Characterization and effects of liquid fraction recirculation

Master's Thesis
2021

88 pages, 34 figures, 18 tables, and 3 appendices

Examiners: Professor Esa Vakkilainen
D.Sc. (Tech) Ekaterina Sermyagina
Supervisors: Professor Esa Vakkilainen
D.Sc. (Tech) Clara Lisseth Mendoza Martinez

Keywords: hydrothermal carbonization (HTC), pulp mill sludge, hydrochar, HTC liquor, recirculation

Hydrothermal carbonization (HTC) is a thermochemical conversion process in which biomass is transformed into a higher quality material with enhanced physical and chemical properties. HTC differs from other techniques in that it uses the moisture present in the biomass to catalyze the reactions, eliminating the need for the energy-intensive drying step. Products formed during HTC can be used in various applications such as energy recovery, soil amendment, and water treatment.

Wastewater and other industrial sludges have grown abundantly in the past years, stimulating a growing interest for environmental and economic disposal methods. In this master's thesis, HTC was applied to pulp mill primary sludge and biosludge, and the liquid fraction of biosludge (HTC liquor) was recirculated up to four times. The results showed that HTC is most effective as a treatment for biosludge in improving its properties for energy and soil amendment. Recirculation did not have a significant effect, meaning HTC liquor could potentially be recycled in HTC to save water.

ACKNOWLEDGEMENTS

Completing this master's thesis has allowed me to grow as a researcher and learn an incredible amount, and I am sincerely grateful to everyone who made my experience possible. First, I would like to thank my supervisor Professor Esa Vakkilainen for supporting me with my Fulbright application even before I arrived in Finland and introducing me to the world of hydrothermal carbonization. Next, I would like to thank my colleagues at Lappeenranta-Lahti University of Technology LUT, especially the Laboratory of Sustainable Energy Systems, for introducing me to the laboratories and equipment. I would especially like to express my gratitude to D.Sc. (Tech) Clara Lisseth Mendoza Martinez for guiding me through daily laboratory work and providing me with invaluable insight while writing. Finally, I would like to thank my family, friends, and partner for sharing endless love and positive energy throughout this process.

Jordan Blake Banks

Lappeenranta,
1 June 2021

TABLE OF CONTENTS

LIST OF FIGURES

LIST OF TABLES

NOMENCLATURE

Abbreviations and chemical formulas

HTC	hydrothermal carbonization
CO_2	carbon dioxide
GHG	greenhouse gases
CH_4	methane
N_2O	nitrous oxide
EU	European Union
FTIR	Fourier-transform infrared spectroscopy
ICP-OES	inductively coupled plasma optical emission spectrometry
HCl	hydrochloric acid
HNO_3	nitric acid
TGA	thermogravimetric analysis
Al_2O_3	aluminum oxide
SEM	scanning electron microscopy
BSE	backscattered electron
XRD	X-ray diffraction
$CaCO_3$	calcium carbonate
H_2O	water
DTG	derivative thermogravimetric

Symbols and parameters

LHV	lower heating value	[MJ/kg]
HHV	higher heating value	[MJ/kg]
BOD	biological oxygen demand	[g/L]
COD	chemical oxygen demand	[g/L]
TOC	total organic carbon	[g/L]
MY	mass yield	[%]
m	mass	[g]
MC	moisture content	[%]
A	ash content	[%]

V	volatile matter	[%]
FC	fixed carbon	[%]
C	carbon content	[%]
H	hydrogen content	[%]
N	nitrogen content	[%]
S	sulfur content	[%]
O	oxygen content	[%]
ED	energy densification	[%]
EY	energy yield	[%]
CI	crystallinity index	[%]
I	diffraction intensity	[counts]
NVR	non-volatile residue	[g, g/kg]
TC	total carbon	[g/L]
IC	inorganic carbon	[g/L]

Elements

Ag	silver	*Mn*	manganese
Al	aluminum	*Mo*	molybdenum
Ca	calcium	*Na*	sodium
Cd	cadmium	*Ni*	nickel
Cl	chlorine	*P*	phosphorus
Co	cobalt	*Pb*	lead
Cr	chromium	*Si*	silicon
Cu	copper	*Ti*	titanium
Fe	iron	*U*	uranium
K	potassium	*V*	vanadium
Mg	magnesium	*Zn*	zinc

1 INTRODUCTION

As countries and industries aim to achieve and exceed sustainability goals, the concept of circular economy – extending the life cycle of products by creating further value from waste – has become attractive (European Parliament, 2021). Pulp production has increased significantly over the years and resultingly, so has its waste, particularly sludge. Stricter regulations require pulp sludge to be treated and utilized rather than landfilled. Instead of being a waste that needs further processing to eventually be discarded, biosludge – one type of pulp mill sludge – has potential as a value-added product, especially for energy and soil applications. Traditionally, biosludge has been difficult to handle due to its high water content as well as complex physical and chemical composition. In recent years, thermochemical conversion processes have been studied due to their ability to upgrade biomass to a material with enhanced properties. Hydrothermal carbonization (HTC) could be a solution for treating biosludge since it uses water present in the biomass as part of the process, mitigating the need for expensive and energy-intensive drying.

The main objective of this thesis is to study opportunities of treating pulp mill primary sludge and biosludge with HTC. Two research questions were proposed:

I. Does treating primary sludge and biosludge with HTC enhance their properties for energy and soil amendment applications?
II. Does recirculating the biosludge liquid fraction after HTC further enhance the properties of the products for energy and soil amendment applications?

These questions will be investigated in the following sections: Section 2 describes the current state of the environment and how biomass can be used to achieve environmental goals. Section 3 explains the pulp mill process and issues related to disposing waste. Section 4 summarizes biomass conversion technologies while Section 5 details HTC. Sections 6 and 7 present the experimental procedures and discuss their results. Section 8 mentions limitations in the experiments and recommends future work. Lastly, Section 9 answers the proposed questions.

2 THE CLIMATE, ENERGY, & BIOMASS POTENTIAL

Over the past two centuries, world energy consumption has increased drastically. Figure 1 shows this exponential rise from about 6,000 TWh in 1800 to nearly 160,000 TWh in 2019. Energy consumption was relatively stable until the early 19th century and then began to rapidly rise in the mid-to-late 19th century, particularly with the additional use of coal, oil, and natural gas during the Industrial Revolution. These fossil fuels contributed 137,000 TWh, or 86% of the consumption, in 2019 (Ritchie & Roser, 2020).

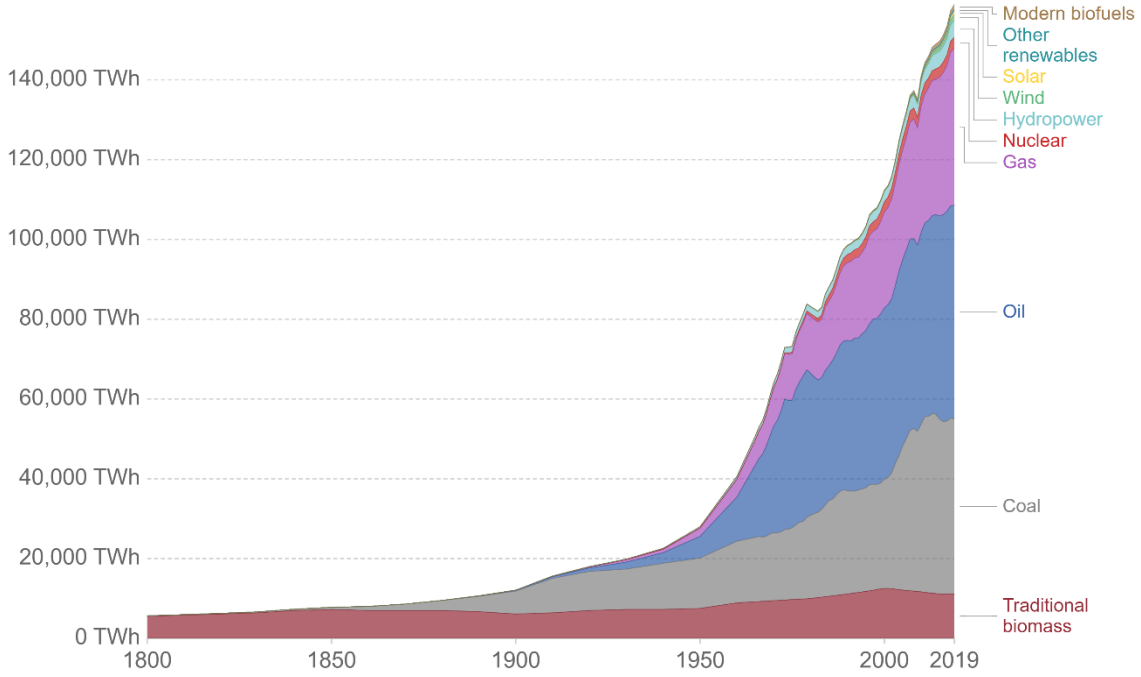

Figure 1. Global direct primary energy consumption by source (Ritchie & Roser, 2020).

Rapid urbanization, economic development, and population growth contribute to higher energy consumption that result in increased carbon dioxide (CO_2) emissions. Figure 2 shows the exponential growth of global CO_2 emissions, from 29 million tons per year in 1800 to 36 billion tons in 2018, with 95% resulting from coal, oil, and gas in 2018 (Ritchie & Roser, 2020).

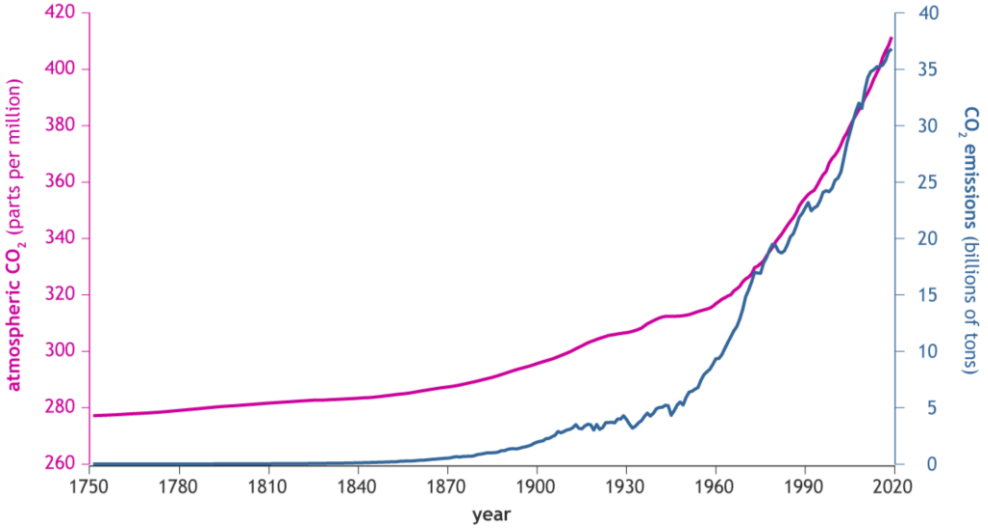

Figure 2. CO_2 in the atmosphere and annual emissions (Lindsey, 2020).

In 2019 the CO_2 level was 410 ppm, the highest in the past 800,000 years. If fossil fuel energy consumption continues as it is projected, atmospheric CO_2 will surpass 900 ppm by 2100 (Lindsey, 2020). CO_2 and other greenhouse gases (GHG) like methane (CH_4) and nitrous oxide (N_2O) trap heat on Earth, causing the average air and sea temperature to rise. As of 2017, the Earth has warmed 1°C due to human activity compared to pre-industrial (1850 – 1900) levels. Temperature rise profoundly affects the environment and its inhabitants through sea level rise, extreme weather, and biodiversity loss. These effects are disproportionately skewed toward impoverished populations, coastal regions, small islands, and big cities in addition to tropical reefs and arctic ecosystems (IPCC, 2018).

To prevent further environmental damage, the 2015 Paris Agreement adopted the goal of limiting the temperature rise to well below 2°C, striving for only 1.5°C if possible (European Commission, 2021b). Holding the temperature at 1.5°C requires CO_2 reduction of 45% by 2030 compared to 2010 levels, which would result in reaching net zero by 2050, while a 2°C limit requires a 25% reduction by 2030 and reaching net zero by 2070. This necessitates "rapid and far-reaching transitions in energy, land, urban and infrastructure (including transport and buildings), and industrial systems" (IPCC, 2018).

According to the United Nations Environment Programme (2020) *Emissions Gap Report 2020*, not enough progress is being made toward the Paris Agreement. In 2019 GHG

emissions grew for the third year in a row, setting a record of 59.1 $GtCO_2e/yr$, where CO_2e is the CO_2 equivalent used to compare various GHG based on their global warming potential (European Commission, 2021a). 38 Gt, or 64% of the year's emissions, were contributed by CO_2. Though CO_2 emissions are predicted to decrease by about 7% in 2020 due to the COVID-19 pandemic, GHG atmospheric concentrations, including CO_2, still increased overall. This will only lead to a 0.01°C reduction in warming by 2050. Less than half of the G20 countries, which produce 78% of all GHG emissions, are on track to achieve their nationally determined contributions under the Paris Agreement. Even if completely fulfilled, global warming could still increase up to 3.2°C by 2100 (United Nations Environment Programme, 2020). In other words, current practices are not sufficient and monumental change is required to prevent an inevitably warmer future.

Fossil fuels are the main contributor to climate change. In 2015, 78.4% of the energy consumption was fossil fuels (REN21, 2017), as shown in Figure 3. Less than 20% came from renewables, and half of that was traditional biomass (i.e. wood fuels, agricultural by-products, and dung burned for cooking and heating purposes). Modern renewables include heat from biomass, geothermal, and solar (4.2%). The aforementioned in addition to wind and hydro are used to generate power (5.2%). Finally, the smallest amount (0.8%) is biofuels used mainly for transport. Renewable energy share has only increased by 1% since the year 2000 (World Bioenergy Association, 2020). Though biomass has been underutilized thus far in modern renewables, it has a significant potential to mitigate the risk of climate change caused by anthropogenic GHG emissions.

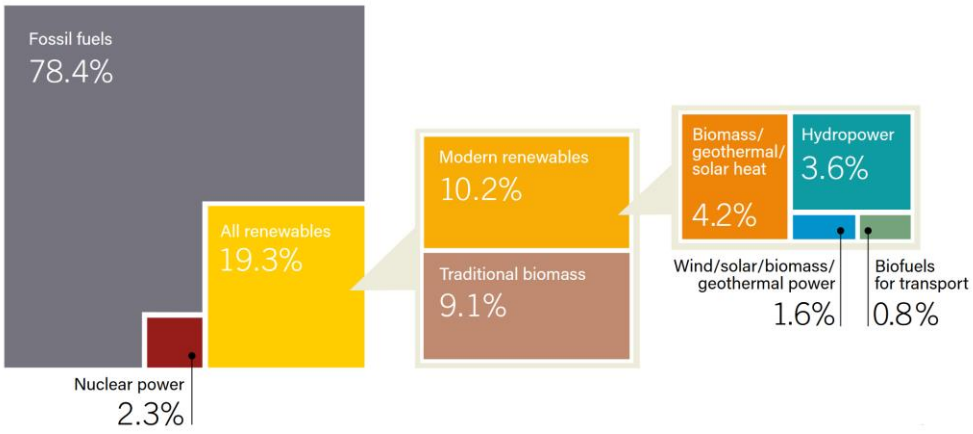

Figure 3. Renewable energy share of total final energy consumption (REN21, 2017).

2.1 Biomass sources

Biomass is organic material derived directly from plants and indirectly through waste. Three sectors – agriculture, forestry, and waste – are typically used to categorize biomass, as detailed in Table 1.

Table 1. Biomass classification (Elbersen et al., 2012; Karp & Halford, 2011).

Sector	Biomass category	Biomass type	Examples
Biomass from agriculture	Energy crops	Grain and seed crops	Corn (stover), wheat (straw), sweet sorghum
		Sugar crops	Sugarcane, sugar beet, sweet sorghum
		Oil crops	Oil palm, soybean, oilseed rape, jatropha
		Dedicated biomass crops	Perennial grasses (Miscanthus, switchgrass, reeds), fast growing trees (willows, poplars)
		Algae	Microalgae, macroalgae
	Agricultural primary residues	Manure	Poultry, sheep, goat, pig, cattle manure
		Solid agricultural residues	Grass, straw, prunnings, orchard residues
Biomass from forestry	Forestry biomass	Woody biomass	Stem wood production, harvested wood
	Primary forestry residues		Felling residues (branches, roots), landscape maintenance residues
	Secondary forestry residues		Wood processing residues (woodchips, sawdust, black liquor)
Biomass from waste	Primary residues	Biodegradable waste	Maintenance activity residues (grass, woody cuttings)
	Secondary residues	Solid, wet agricultural residues	Processing residues (pits, shells, slaughter waste)
	Tertiary residues	Biodegradable waste	Organic household waste (food, paper, furniture)
		Organic waste from industry, trade	Woody fractions, packaging, demolition wood
	Waste biomass	Biodegradable waste	Sewage sludge
		Mixed waste	Municipal solid waste

Although dedicated biomass crops often grow quickly and have a high energy content, they provoke the food versus fuel debate. These crops require resources such as land, water,

energy, and nutrients to grow. This land could be used to grow food for the rapidly multiplying population instead. Furthermore, clearing land for energy crops may have environmental implications like biodiversity loss, water depletion or contamination, and releasing stored CO_2 (Karp & Halford, 2011). One emerging area of study is using marginal land to grow energy crops. This is land that is unsuitable for food production, lower quality, or not productive for agriculture (Shortall, 2013). One analysis estimates that using marginal land can increase energy crop biomass potential by 30 to 45% (Dornburg et al., 2010). Marginal land use is more environmentally friendly but requires significant research and implementation before becoming economically feasible. To avoid this controversy and improve sustainability, using waste and residues for bioenergy production is ideal.

As shown in Figure 4, 67% of biomass feedstock for bioenergy is fuelwood. Including residues, wastes, and processed wood, 87% of biomass originates from the forest. The next largest source at 10% is agriculture, consisting of animal and agricultural by-products as well as energy crops. Lastly there is municipal solid waste and landfill waste accounting for 3%.

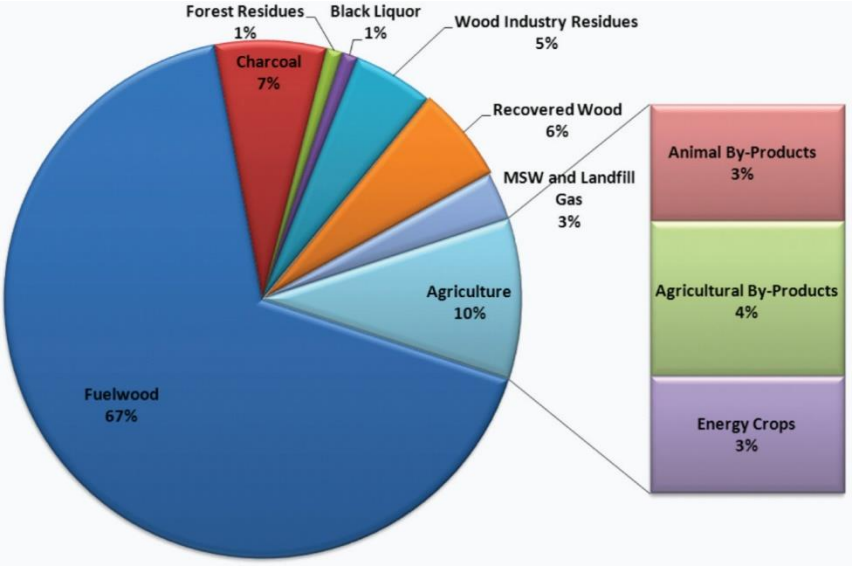

Figure 4. Biomass feedstock sources (Karaca & Erdoğdu, 2013).

Furthermore, typical biomass and coal combustion properties are listed in Table 2. Coal has a heating value 1 to 3 times that of biomass due to its considerably higher fuel density and carbon content. Biomass also generally has higher moisture, particle size, oxygen, silica, and

potassium, but lower aluminum and iron than coal. High volatility and reactivity give biomass an advantage as a fuel, but it is often co-fired with coal due to its less favorable properties (Demirbas, 2004).

Table 2. Physical, chemical, and fuel properties of biomass and coal (Demirbas, 2004).

Property	Biomass	Coal
Fuel density (kg/m^3)	~500	~1300
Particle size	~3 mm	~100 μm
C content (wt% of dry fuel)	42–54	65–85
O content (wt% of dry fuel)	35–45	2–15
S content (wt% of dry fuel)	Max 0.5	0.5–7.5
SiO_2 content (wt% of dry ash)	23–49	40–60
K_2O content (wt% of dry ash)	4–48	2–6
Al_2O_3 content (wt% of dry ash)	2.4–9.5	15–25
Fe_2O_3 content (wt% of dry ash)	1.5–8.5	8–18
Ignation temperature (K)	418–426	490–595
Peak temperature (K)	560–575	–
Friability	Low	High
Dry heating value (MJ/kg)	14–21	23–28

2.2 Bioenergy

Bioenergy is the largest contributor to renewable energy, making up 67% of renewables, or 56 EJ, in 2018. The main use of biomass is heating. In 2018, 96% of renewable heat was derived from biomass. Additionally, biomass accounted for 91% of renewables in transport but only 9% of renewable electricity (World Bioenergy Association, 2020).

Chum, Faaij, & Moreira (2011) projected an 80 to 90% emission reduction with bioenergy compared to fossil fuels when a highly developed system of perennial energy crops, biomass residues and wastes, and advanced conversion is implemented. For example, ethanol from

corn, sugarcane, corn stover, switchgrass, and miscanthus could reduce GHG emissions by 19–48%, 40–62%, 90–103%, 77–97% and 101–115%, respectively, when compared to petroleum gasoline (Wang et al., 2012). However, reductions could be negated if land use change and forests are not effectively managed. Though the ranges vary widely, bioenergy is a suitable means of reducing overall emissions.

There are several different scenarios for how much biomass could be produced for bioenergy. Smeets et al. (2007) categorized these potentials in five categories: theoretical, geographical, technical, economic, and implementation, in order of largest to smallest potentials. Theoretical potential is the upper limit restricted by physical and biological barriers, including both land and water. Next is geographical only considering land area. On land, technical depends on the advancement of agricultural technology but is not limited by food production, housing, infrastructure, and forest conservation. Subsequently, economic involves the economically profitable technical potential. Finally, implementation factors in timeframes, social constraints, and policy incentives. Most studies make estimates starting at technical potential because theoretical and geographical are not feasible in any case. In a later study, Batidzirai, Smeets, & Faaij (2012) removed geographical potential and added ecologically sustainable potential. As seen in Figure 5, some of these potentials can overlap. For example, a biomass potential may be ecologically sustainable but economically unfavorable. It is notable to mention that various studies may utilize potentials with the same name but different definitions.

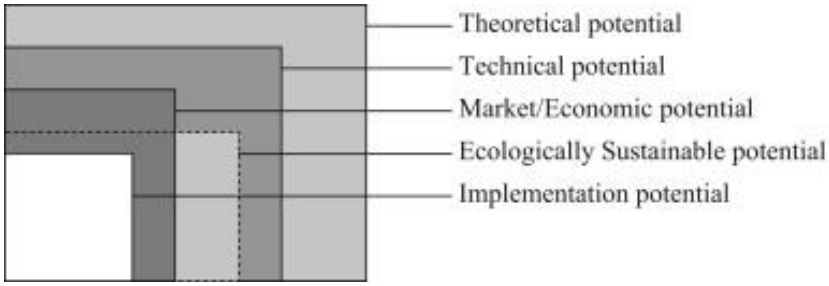

Figure 5. Overlapping biomass potential (Batidzirai, Smeets, & Faaij, 2012).

Chum, Faaij, & Moreira (2011) compiled the technical potentials shown in Table 3. The total global technical potential may vary widely from less than 50 to more than 1000 EJ/yr. Though not likely, the biomass potential could be less than the current consumption if there

is high food and fiber demand along with slow land productivity development. While the forest currently accounts for about 90% of bioenergy production, this could shift to nearly 70% from agriculture in 2050.

Table 3. 2050 biomass global technical potentials (Chum, Faaij, & Moreira, 2011).

Biomass category	**Technical potential** (EJ/yr)
Residues from agriculture	15 – 70
Dedicated biomass production on surplus agricultural land	0 – 700
Dedicated biomass production on marginal lands	0 – 110
Forest biomass	0 – 110
Animal manure	5 – 50
Organic wastes	5 – > 50
Total	**< 50 – > 1000**

Smeets et al. (2007) and Dornburg et al. (2010) predicted the highest technical biomass potential in 2050 to be about 1500 EJ/yr. Both rely on the intensive technological development of agricultural systems and growing energy crops on surplus agricultural land. On the other hand, Chum, Faaij, & Moreira (2011) stated a more conservative upper technical bound of 500 EJ/yr. In terms of environmental and societal sustainability, these estimates are reduced to more practical potentials of 100 to 300 EJ/yr (Chum, Faaij, & Moreira 2011) and 200 to 500 EJ/yr (Dornburg et al., 2010). Factors affecting biomass potential include biodiversity effects, water availability and use, food demand and production, agro-economic models, food prices, market, policy, and technological development.

3 PULP

In 2018 the global production of wood pulp was 188 million tons, an increase of 49% since 1980 (FAO, 2020). As seen in Figure 6, North America dominates the industry, making up 38% of the world pulp production, with Europe trailing behind at 10% less. In the past years, pulp production has grown rapidly due to Asia and South America increasing their contribution in the 1990s, a total of 17 and 13%, respectively, in 2013. Today, Oceania and Africa still only produce a nominal amount of pulp.

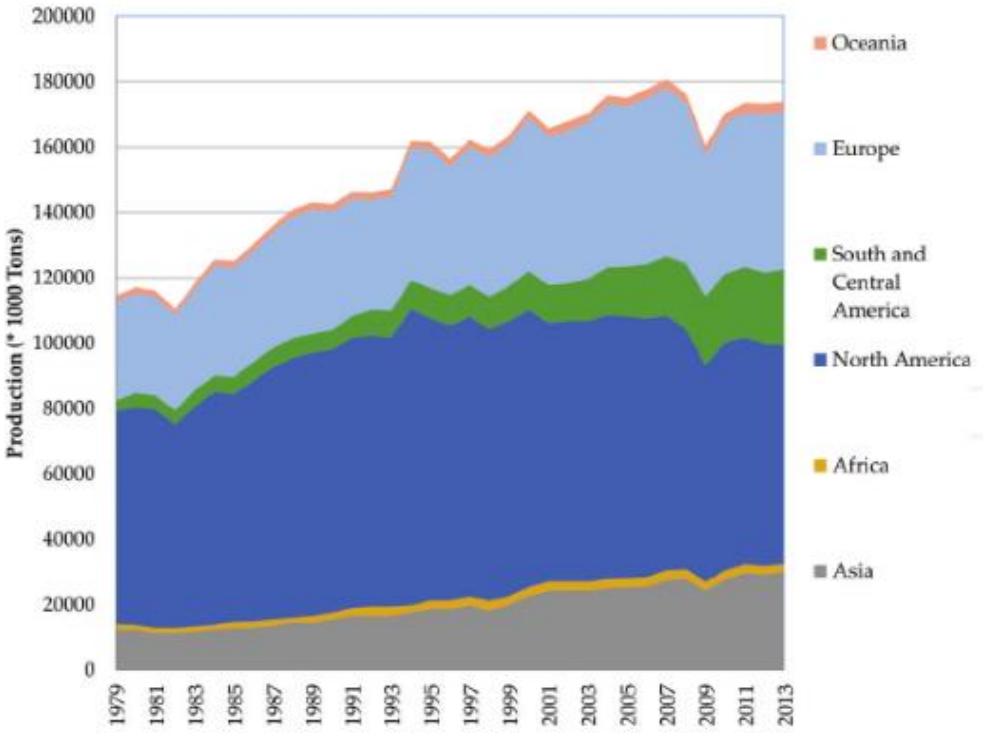

Figure 6. World pulp production 1979-2013 (Cabrera, 2017).

3.1 Pulp production

In a pulp mill, organic material is broken down into cellulosic fibers that can be used as a raw material for paper, boards, and other products. Pulp can be derived from any fibrous plant such as wood, straw, or grass, but wood is the most common type. The cellulosic fibers can be separated by mechanical, semi-chemical, or chemical processes (Gavrilescu, 2013). In mechanical pulping, mechanical energy is used to separate fibers. For example, logs or wood chips are ground or steamed under pressure and elevated temperature. This results in a high yield of 90 to 98% and is often used for newspaper and magazine paper. Furthermore,

semi-chemical pulping involves both moderate chemical and mechanical treatment, resulting in a pulp yield of 60 to 80% suitable for corrugated medium. Lastly, chemical pulping utilizes chemicals, high temperature, and pressure to degrade and dissolve lignin, producing the lowest pulp yield of 45 to 55%. Chemical pulping comprises two-thirds of total pulp production and is the highest in strength, used for printing, writing, packaging, and paperboard (Gaines, 2004). Pulp production includes the generation of various waste streams, which require special disposal due to the nature of their composition. One waste in particular, sludge, will be the focus of this study.

3.2 Sludge

Sludge is the solid by-product of wastewater treatment in pulp and paper as well as other industries. Europe, the United States, and China alone generate an average of nearly 250 million wet tons of sludge per year (Pritchard et al., 2010). Sludge often makes up half of the operating costs in wastewater treatment plants and is typically disposed of by landfill, agricultural use, or incineration, which cost 30 – 100€ per wet ton in Europe (Bhatt et al., 2018; Pritchard et al., 2010). Due to expensive disposal as well as regulations on landfilling organic waste, in recent years there has been substantial research to find alternative uses.

Sludge results from the wastewater generated in pulp and paper production. In the two-step process shown in Figure 7, wastewater passes through the primary and secondary clarifiers, producing primary and secondary sludge – often called biosludge – respectively.

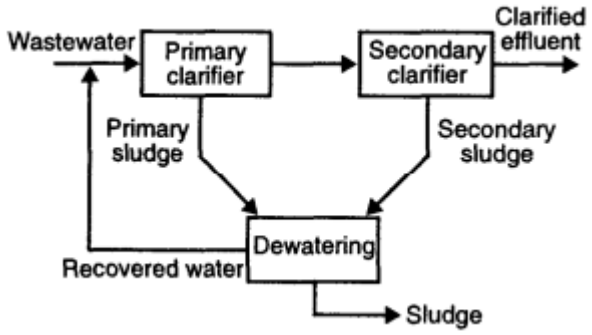

Figure 7. Pulp and paper mill wastewater treatment (Scott et al., 1995).

The most common method for primary clarification is sedimentation, where solids, or primary sludge, settle to the bottom of a tank and are removed. Primary sludge is mainly composed of cellulose and hemicellulose fibers. The overflow from the primary clarifier is then pumped through the secondary clarifier, where micro-organisms consume the waste and oxygen, releasing carbon dioxide and water as well as solids, or biosludge, that settle to the bottom (Scott et al., 1995; Rodrigues et al., 2021). Biosludge is a combination of microorganisms, unsettled fibers from the primary tank, undigested organics, inorganic material, and concentrated metals (Kuparinen et al., 2019). Properties of various types of sludge from pulp and paper mills are listed in Table 4 and more extensive properties of biosludge in Table 17 of Appendix 1.

Table 4. Pulp and paper mill sludge properties (Lohiniva, Mäkinen, & Sipilä, 2001).

		Pulp mill sludge-mix	**Primary sludge**	**Paper mill sludge-mix**	**Biosludge**	**Deinking Sludge**	**Debarking sludge**
Moisture	%	75 - 80	70	--	85	60	70
Ash		1321	25 - 60	12 - 20	16	30 - 60	2.5
C		40 - 42	44	44 - 46	47	25 - 45	50
H		4.5 - 5.0	6	5.5-6.0	5.2	4 - 5.5	6
S		0.4 - 1.3	0.1	0.05 - 0.1	1.2	0.1 - 0.3	0.02
N		1.3 - 2.9	0.4	0.5 - 0.7	1.6	0.1 - 0.3	0.8
O		25 - 29	25	--	30	22	34
Cl		0.1 - 0.8	--	0 - 0.1	0.04 - 1.5	0.2 - 0.6	--
LHV	MJ/kg	14 - 18	2.3	--	17.4	8 - 13	--

Various sludge disposal methods and applications include landfill, fertilizer, incineration, and supplements in other products like fillers. Incineration, which costs 13 – 15 USD per dry ton, is becoming the most common method due to European Union (EU) waste directives, such as landfilling of biodegradable waste being prohibited (Saha et al., 2019; Kuparinen et al., 2019). Before being effectively combusted, the moisture content of sludge must be reduced. Sludge can be dewatered by methods such as pressing and centrifuging. Thermal drying is possible but is expensive and energy intensive. Primary sludge can be combusted in boilers for additional energy due to the high amount of fibers and easy dewaterability. On the other hand, high moisture content and gel-like structure make biosludge difficult both to dewater and incinerate (Meyer et al., 2018).

In 2016 the EU-28 generated nearly 8.5 million tons of sludge from treating wastewater (European Commission, 2020). Sludge production as well as treatment varies widely between Member States. For example, in 2005 the EU-15 (old Member States) produced 21.9 kg per p.e. (population equivalent) of sludge whereas the EU-12 (new Member States) produced 11.5 kg per p.e. due to differences in centralized wastewater treatment systems and treatments (Kelessidis & Stasinakis, 2012). The most common sludge treatment methods in the EU are anaerobic and aerobic digestion, which are used by 89% and 75% of countries, respectively, with a minor amount applying chemical stabilization. Afterward, 50% of sewage sludge is spread on agricultural land, 28% incinerated, and 18% disposed in landfills, which also varies by Member State, seen in Figure 8 (Collivignarelli et al., 2019). Outside of the EU, in 2013 China produced 6.25 million tons of dry solids, 80% of which was disposed by improper dumping (Yang et al., 2015), and in 2015 52% of pulp and paper mill sludge was landfilled in the United States (Faubert et al., 2016).

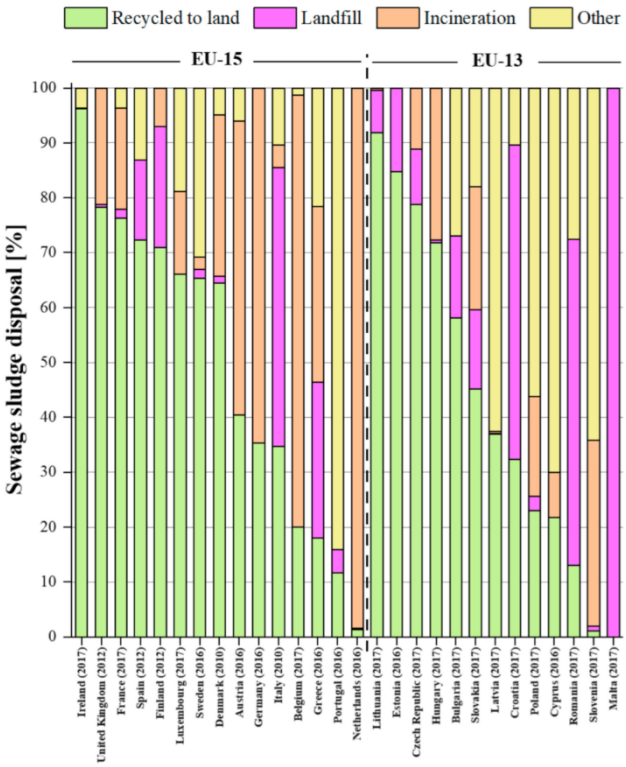

Figure 8. Sewage sludge recovery routes in the EU (Collivignarelli et al., 2019).

While the most convenient path for biosludge produced in a pulp or paper mill would be incineration, it usually has a moisture content above 98%, which leads to a negative lower heating value unsuitable for combustion (Meyer et al., 2018; Kuparinen et al., 2019). According to Vesilind & Martel (1989), biosludge contains four types of water, shown in Figure 9. Free water is detached from solids and can be separated by gravitational settling. Interstitial water is trapped within a floc and is released by mechanical dewatering such as centrifugation when the floc is broken, or the cell is destroyed. Vicinal water is physically bound to the cell's surface and cannot be separated by mechanical means. Finally, hydration water is chemically bound to the cell's surface and can be released by thermochemical treatment (Mowla, Tran, & Allen, 2013).

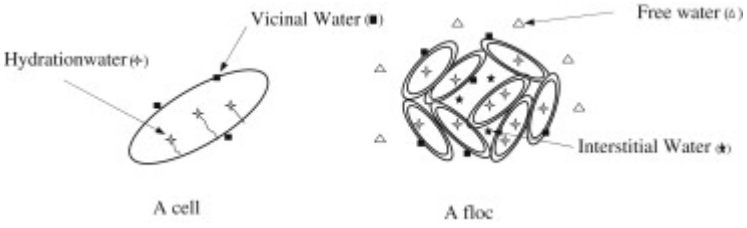

Figure 9. Forms of water in biosludge (Mowla, Tran, & Allen, 2013).

In order to improve its properties, biosludge is often mixed with primary sludge. Without pretreatment, biosludge mixed with primary sludge, thickened, and dewatered with a screw press has 30-40% solids, as compared to alone having a solids content below 20%. Though the sludge ratio varies between mills, the average Canadian mill produces 70% primary sludge and 30% biosludge (Meyer et al. 2018). Thus, primary sludge is abundant in mills and it could be beneficial to add some to biosludge while leaving enough to be combusted in the boiler to offset energy costs. Furthermore, a study of five enzymes showed that lysozyme acts as a flocculant, allowing for enhanced biosludge dewaterability and increased solids content (Bonilla, Tran, & Allen, 2015).

4 BIOMASS CONVERSION

There are various methods to convert biomass into bioenergy, depending on the type of biomass and the desired form of energy. Figure 10 shows the common feedstocks, conversion routes, and end products. These conversion routes can be further classified as biological, chemical, or thermochemical. Biological includes fermentation and anaerobic digestion while chemical includes transesterification. Additionally, pelletizing – or densifying – biomass can be considered a conversion or upgrading method. In this section the pyrolysis, gasification, and torrefaction thermochemical techniques are discussed.

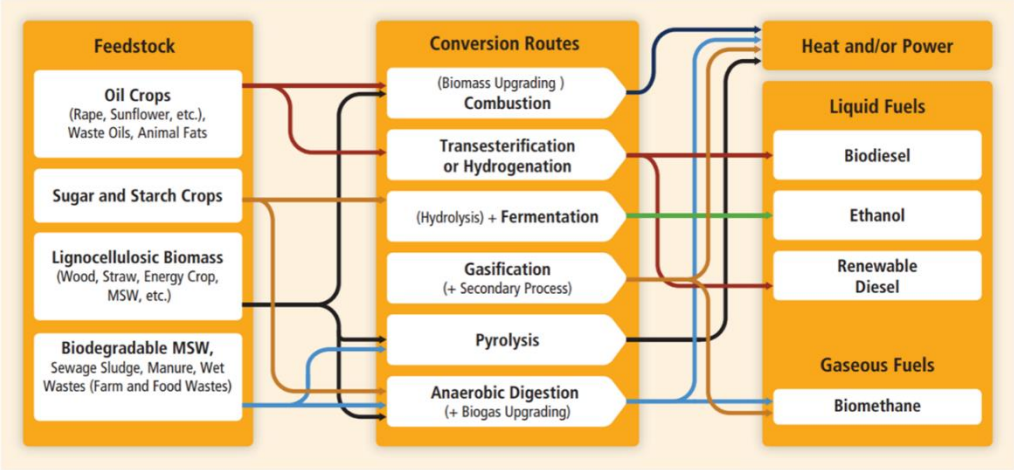

Figure 10. Commercial bioenergy routes by (Chum, Faaij, & Moreira, 2011).

4.1 Pyrolysis

Pyrolysis is the decomposition of biomass in the absence or limitation of oxygen. In this process, rapid heating breaks down large hydrocarbon molecules into gas (70 – 90 wt%), liquid (1 – 20 wt%), and solid (5 – 25 wt%) components. The typical temperature range is between 300 and 650°C, and it is a precursor to gasification. Pyrolysis products include biochar, condensable gases that condense into bio-oil, and noncondensable gases that are captured in gaseous form (Molino, Chianese, & Musmarra, 2016). Considering biomass with an initial lower heating value (LHV) of 19.5 to 21 MJ/kg, bio-oil has a lower LHV of 13 to 18 MJ/kg, while biochar has a higher LHV of about 32 MJ/kg. Pyrolysis gas has an LHV of 11 to 20 MJ/Nm^3. Furthermore, pyrolysis can be classified as slow or fast. Slow pyrolysis is the oldest form that has been used for thousands of years, in which biomass is heated slowly

at a low temperature (400 to 600°C) to primarily produce charcoal or char. On the other hand, fast pyrolysis rapidly heats biomass at a rate of 1000 to 10,000°C/s up to 650°C for bio-oil or even 1000°C if gas is the desired product. Slow pyrolysis residence time is on the order of minutes while fast pyrolysis is on the order of seconds. The most influential characteristics affecting pyrolysis are the pyrolyzer design, type of biomass, heating rate, final temperature, and residence time (Basu, 2013).

4.2 Gasification

Gasification is another thermochemical conversion process in which gas is the main product. The steps of gasification include biomass drying, thermal decomposition, partial combustion of gases, vapors, and char, and finally gasification of the decomposed products (Basu, 2013). As mentioned previously, gasification builds upon pyrolysis which further utilizes a gasifier such as air, oxygen, steam, or carbon dioxide to partially oxidize the carbon in the biomass. The typical temperature range is 800 to 1100°C, and like in pyrolysis, heavily affects the product yields. Gasification produces syngas, which is made up of mainly carbon monoxide, hydrogen, methane, and carbon dioxide as well as heavy and light hydrocarbons. Syngas has an LHV of 4 to 13 MJ/Nm^3, a bit lower than pyrolysis gas. Tars are condensable hydrocarbons present in the syngas that can negatively affect the use of syngas and are often difficult to remove (Molino, Chianese, & Musmarra, 2016).

4.3 Torrefaction

Torrefaction is the partial decomposition of biomass in the absence of oxygen. During torrefaction, hemicellulose breaks down, bonding the cellulose fibers, and cellulose depolymerizes, decreasing the length of the fibers. The change in composition transforms the biomass into a brittle and easy to grind material. Most of the mass and energy yield is distributed in the solid product, with a smaller percentage in water, gases, organics, and lipids. The method utilizes operating temperatures between 200 and 300°C and a low heating rate of under 50°C/min (Bergman & Kiel, 2005). Torrefaction often increases the LHV from between 17 and 19 MJ/kg to between 19 and 23 MJ/kg but can even reach 30 MJ/kg under complete devolatization. This is primarily due to the removal of oxygen-containing light volatiles. Thermal energy generated by the combustion of torrefaction gases is often used to dry the incoming biomass since it should not exceed 15% moisture (Cremers et al., 2015).

5 HYDROTHERMAL CARBONIZATION

The main topic of this thesis, hydrothermal carbonization (HTC), will be discussed in terms of the reaction process, applications, and recirculating its liquid fraction.

5.1 Process

HTC is an emerging thermochemical process in which biomass is heated in the presence of water to convert it to a higher quality material. Unlike the other thermochemical processes, HTC relies on the biomass moisture instead of evaporating it, using the water as a solvent at the high temperatures and pressures (Saha et al., 2019). Thus, the energy required for this aspect is lower, reducing consumption and costs. One study found that hydrothermally treating sewage sludge required less energy than conventional drying. The reaction is carried out between 180°C and 250°C with residence times widely ranging between five minutes and six hours and pressures up to 5 MPa (Bhatt et al., 2018).

5.1.1 Reaction mechanism

HTC reactions hydrolyze and dehydrate the cellulose, hemicellulose, and lignin in biomass into monosaccharides and disaccharides. These carbohydrates undergo dehydration, hydrolyzation, and decarboxylation to form intermediates that are condensed into hydrochar (Tasca et al., 2019), depicted in Figure 11. Resulting products include 50-80% solids (hydrochar), 5-20% liquids (HTC liquor), and 2-5% gases (Kuparinen et al., 2019).

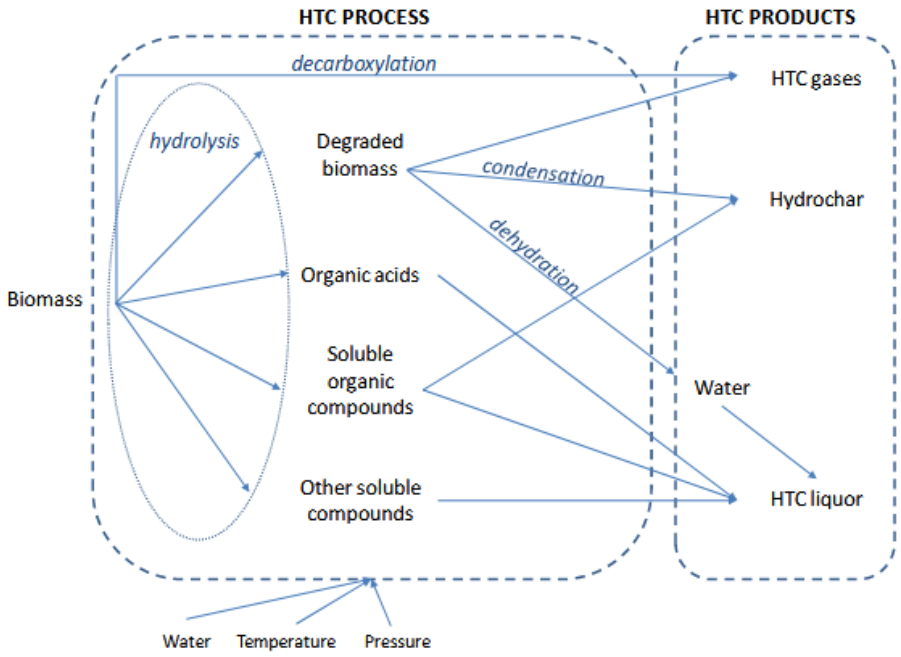

Figure 11. HTC process (Langone & Basso, 2020).

5.1.2 Parameters

Temperature has the most significant effect on HTC process severity, followed by water-to-biomass ratio and even less by residence time (Mendoza Martinez et al., 2021). Type of biomass also plays an important role because different components behave differently during the HTC reactions. Increasing the reaction temperature of HTC decreases the hydrochar mass yield but increases the liquid and gas fractions. This occurs because cellulose and lignin require higher temperatures to degrade, while hemicellulose degrades at a lower temperature. Furthermore, higher heating value (HHV) increases between hemicellulose, cellulose, and lignin. Since more lignin remains at higher temperatures, the overall HHV will be higher (Heidairi et al., 2019). Additionally, biomass can be treated with acids before performing HTC. Hydrochar with lower pH may have increased carbon content, mass yield, and heating value as well as larger surface area, pore volume, and pore size, which enhance heavy metal adsorption (Ameen et al., 2021; Reza et al., 2015; Khoshbouy et al., 2018).

5.1.3 Properties

The properties of hydrochar vary widely depending on type of biomass and HTC treatment. A review of lignocellulosic hydrochar solid properties is presented in Table 5. Mass yields

vary between 30 and 80%, carbon content between 40 and 70%, and ash content between 0.5 and 25%. HHV ranges from 18 to 29 MJ/kg, while H/C and O/C ratios are between 0.3 and 1.6 (Heidari et al., 2019).

Table 5. Effects of HTC on solid properties of various feedstocks (Heidari et al., 2019).

Feed	Temp. (°C)	Time (min)	Solid mass yield (%)	Carbon content (%)	Ash content (%)	HHV (MJ/Kg)	H/C ratio	O/C ratio
Lawn grass	200	180	48	45	-	19	1.5	0.45
Lawn grass	240	180	32	55	-	20.8	1.2	0.4
Corn husk	260	15	33.2	63.41	3.74	27.66	1.1	0.3
Bambu	190	20	48	56.5	-	21	1.27	0.6
Cellulose	220	30	58.4	63.5	1.4	26.5	0.9	0.36
Wheat straw	260	360	35.7	64.2	10.8	26.2	1.02	0.22
Grape pomace	275	30	48	68.32	2.7	28.31	1.01	0.25
Miscanthus	180	240	80	53.5	1.75	21.2	1.33	0.55
Miscanthus	200	240	65	56.6	0.88	21.4	1.25	0.48
Miscanthus	220	240	58	63	1.05	23.9	1.1	0.36
Miscanthus	200	120	65	54.9	1.75	21.1	1.29	0.51
Miscanthus	200	720	65	58.7	0.83	23.4	1.24	0.25
Rice husk	200	360	65	40.81	24.54	15.7	1.3	0.39
Saw dust	240	30	49.45	-	0.84	24.5	-	-
Loblolly pine	230	120	63.65	-	0.5	22.7	-	-
Sugarcane Bagasse	175	30	69.6	48.3	-	18	1.41	0.72
Sugarcane Bagasse	215	30	67.7	48.4	-	19.7	1.19	0.56
Loblolly pine	175	30	77.7	52.2	-	21	1.38	0.58
Loblolly pine	215	30	72.4	54.8	-	22.1	1.55	0.54

Table 6 presents HTC liquor properties when different feedstocks and parameters are considered. Mäkelä et al. (2018) studied the behavior of the HTC liquid fraction of sludge treatment, reporting that adding chemical sludge HTC filtrate back to a pulp and paper mill wastewater treatment plant would increase the suspended solids, biological oxygen demand (BOD), chemical oxygen demand (COD), and total nitrogen by up to 0.8, 5.3, 3.1, and 67%, respectively. Therefore, additional filtrate treatment would be necessary for an HTC pulp and paper mill integration. Higher HTC temperatures decrease the amount of suspended solids and enhance filtrate biological decomposition, aiding the biological treatment process.

Table 6. Effects of HTC on liquid properties of various feedstocks (Usman et al., 2019).

Feedstock	Operating conditions [a]	HTC-AP yield (%) [b]	pH	COD ($g\ L^{-1}$)	TOC ($g\ L^{-1}$)	TN ($g\ L^{-1}$)	TP ($g\ L^{-1}$)
Corn silage	T: 220 °C; RT: 6 h; SL: 4.3%	—	3.8	41.4	15.7	0.7	0.2
Sugar beet waste	T: 338 °C; AF SL: 14.1%	55	4.7	110.4	—	—	—
Pine; corn stover	T: 350 °C; SL: 9.6–14.5%; FR: 1.0–1.5 L h^{-1}; P: 20.7 MPa	27.7–45	4.4–5.4	40.0–74.0	—	—	—
Rice straw	T: 170–330 °C; SL: 9.6–14.5%; RT: 30 min	12.11–30.96	3.7–5.6	14.3–29.0	3.9–10.3	—	—
Extracted grain waste	T: 331 °C; AF SL: 12.8%; P: 20.1 MPa; FR: 4.0 L h^{-1}	26	6.2	55.9	—	—	—
Poplar wood chips	T: 220 °C; S/L: 20/100; RT: 4 h	15	3.4	50	17.4	—	—
Algal	T: 260–350 °C; RT: 30–90 min; SL: 10–20%	4–88	7.5–9.0	23.0–160.0	23.2–35.0	11.0–31.7	0.7–1.9
Grapes and pomace waste	T: 175–349 °C; RT: 30–120 min; P: 20.0 MPa	29–42	7.5	57.0–84.7	21–26	—	—
Sewage sludge	T: 140–320 °C; RT: 15–240 min; SL: 2.4%	2–57	—	17.5–105.6	4.9–13.7	—	—
Municipal sludge	T: 225–275 °C; RT: 15–60 min	27–67	—	—	2.487	0.514	0.048
Digested sludge	T: 350 °C; AF SL: 11.5%; P: 20.0 MPa; FR: 1.5 L h^{-1}	26	8.0	48.2	—	—	—
MSW pulp and digestate	T: 200–300 °C; RT: 30, 120 min; S/L: 40/100	1.3–6.9 g/100 g	4.3–9.2	12.2–12.6	0.39–4.9	0.1–2.4	0.10
Oleaginous yeast	T: 345 °C; AF SL: 14.9%; P: 20.0 MPa; FR: 1.5 L h^{-1}	21	4.1	59	—	—	—

[a] T: temperature; AF: ash-free; SL: solid load; P: pressure; FR: feed rate; S/L: solid/liquid mass ratio; RT: residence time. [b] Based on the carbon percentage.

5.2 Applications

The products of HTC can be used for various applications. These include energy, soil amendment, separation of pollutants from flue gas streams, adsorption of heavy metals and contaminants from water, chemical recovery, and algae cultivation (Heidari et al., 2019; Usman et al., 2019). This study will focus on energy and soil amendment.

5.2.1 Energy

Hydrochar is a coal-like substance with a higher heating value than untreated biomass. In comparison, the heating value of fossil coal is about 30 MJ/kg and the heating value of HTC biosludge is above 20 MJ/kg, while it is low, about 0.5 MJ/kg or sometimes even negative, for untreated biosludge (Kuparinen et al., 2019). Hydrochar can be combusted in the boiler for additional energy. Additionally, HTC liquor, often high in nutrients, can be anaerobically digested to produce biogas. Biogas can generate electricity or be upgraded to biomethane, which is used for vehicles or piped to the natural gas grid (Langone & Basso, 2020). Ferrentino et al. (2020) found, based on laboratory tests and simulation, that biomethane yield doubled when HTC liquor was digested with primary and secondary sludge, compared to the sludge alone, and increased by over three times when hydrochar was included. However, Wang et al. (2018) observed that hydrothermally pretreated rice straw anaerobic

digestion improved only marginally at low temperatures and was prohibited at high temperatures, suggesting that type of biomass and temperature play a significant role.

5.2.2 Soil Amendment

Furthermore, hydrochar has a high carbon content, nutrient level, and heavy metal absorption, making it ideal for land use. Mohammadi et al. (2019) performed an environmental analysis showing that pulp and paper mill biosludge biochar is preferable for soil amendment than energy recovery. Eskandari et al. (2019) found that growing pine tree seedlings in 20% hydrochar with a 50% liquid fertilizer rate had a similar quality, nutrient, and heavy metal uptake as those grown with a 100% fertilizer rate, indicating that hydrochar can reduce fertilizer requirements. Currently almost all of Europe's phosphorus, an essential element for agricultural and industrial uses, is imported. Therefore, HTC liquor has great potential for reclamation due to its high amounts of ammonium and phosphate (Langone & Basso, 2020). The addition of hydrochar generally increases soil pH, promoting the mass production of plants, but can also have negative effects such as reduction of mineral N content in the soil as well as in the plant if the hydrochar has a high C: N ratio. Thus, it is important to understand the soil and plant growth requirements as well as the hydrochar effect before application (Bargmann et al., 2014).

5.2.3 Industrial utilization

Though the technology is promising, there are only a few examples of industrial utilization of HTC to date, five of which are detailed in Table 7.

Table 7. Industrial HTC applications. (See company name for reference.)

Company, country	Start date, technology	Biomass	Products
Ingelia, Spain	2007: developed technology 2010: industrial prototype 2015+: plants in Spain, Italy, United Kingdom, Canada, Belgium, and Portugal	Various	Biocoal, liquid fertilizer
SunCoal, Germany	2008: CarboREN 2013: CarboBoost	Various	Biocoal, syngas, technical and activated carbons
HTCycle, Germany	2010: industrial-scale plant 2017: second plant	Agricultural waste, sewage sludge	Biocoal, phosphorus and ammonia sulphate recovery, activated carbon for wastewater adsorption
TerraNova Energy, Germany	2016: TerraNova® Ultra operational plant in China (40,000 tons of sewage sludge annually)	Sewage sludge	Biocoal, biogas, phosphorus
C-Green, Sweden	2020: OxyPower HTC integrated at Stora Enso's paper mill in Finland (16,000 tons of sludge annually)	Paper mill biosludge	Biocoal, biogas, nitrogen and phosphorus recovery

5.3 Recirculation

According to Xu et al. (2020), the most common methods of disposing sewage sludge HTC liquor are anaerobic digestion, wet oxidation, algae cultivation, and recycling. Since HTC is such a water-intensive process, the idea of recirculating liquor has been explored for its water, energy, and nutrient recovery benefits. After HTC and filtration, the liquor is used again in the next round of HTC – in the place of fresh water – with new biomass. The major effects of recirculation on the hydrochar are the increase in dewaterability, mass, and energy yield due to enhanced dehydration and deposition of degraded polymers onto the formed porous surface (Tasca et al., 2019). Organic acids generated in HTC can catalyze hydrolysis and decarboxylation when recirculated, improving the content of the hydrochar as well as CH_4 production if treating the liquor with anaerobic digestion (Mäkelä et al., 2018; Wang et

al., 2019). Additionally, Stemann & Ziegler (2011) simulated that recirculating hot compressed HTC liquor can be an efficient method of recovering heat and reducing the heating requirement in an HTC plant by ten times.

Table 8 summarizes the hydrochar results of four HTC recirculation studies. Various conditions and dilutions of HTC liquor were used in the recirculation experiments. From the studies it is apparent that additional recirculations do not necessarily increase the mass yield and HHV any higher. Usually there is a peak between the third and sixth recirculation.

Table 8. Hydrochar recirculation properties.

Reference	**Biomass**	**HTC conditions**[1]	**Recirculation conditions**[2]	**Mass yield** (%)	**HHV** (MJ/kg)
Wang et al. (2019)	Macroalgae *Laminaria*	w:b = 20:1 t = 2 h T = 220°C	12 r 100%	13.3 – 17.8	18.4 – 22.7
Kambo, Minaret, & Dutta (2018)	*Miscanthus*	w:b = 6:1 t = 0.08 h T = 260°C	10 r 17%	47 – 57	26.06 – 26.64
Xu et al. (2020)	Sewage sludge from a municipal wastewater treatment plant	w:b = 1:1 -- T = 200°C	5 r 100%	72.0 – 73.5	6.88 – 8.67
		T = 230°C		68.5 – 67.5	8.44 – 8.75
		T = 260°C		65.3 – 64.4	7.59 – 8.12
Zhang et al. (2020)	Sewage sludge from a municipal wastewater treatment plant	w:b = 10:1 t = 1 h T = 220°C	4 r --	69.87 – 73.80	5.74 – 7.23
	50% water hyacinth and 50% sewage sludge			63.20 – 67.00	12.89 – 13.87

1: w:b – water to biomass ratio, t – time, T – temperature

2: r – recirculation; % of water requirement that is HTC liquor

Furthermore, literature data for HTC liquor recirculation are presented in Table 9. Wang et al. (2019) found that COD increased nearly 8 times when HTC liquor was recirculated 12 times and about 4 times after 4 recirculations. Zhang et al. (2020) also observed increasing COD and total organic carbon (TOC) after recirculation as well as negligible change in trace elemental concentration, including Ca, Mg, Al, Cd, and Pb. Xu (2020) measured a COD

increase of 1.43 times at 220°C after 4 recirculations but only 1.23 times at 240°C. Additionally, biogas yield decreased after each recirculation due to accumulation of anaerobic digestion inhibitors, such as furfural, in the HTC liquor. On the other hand, Köchermann et al. (2018) identified that the COD/TOC ratio decreased with each recirculation, indicating an accumulation of carboxylic acids, which are precursors of several industries that could add value if recovered (Wainaina et al., 2019).

Table 9. HTC liquor recirculation properties.

Reference	**Biomass**	**HTC conditions**[1]	**Recirculation conditions**[2]	**COD** (g/L)	**TOC** (g/L)
Wang et al. (2019)	Macroalgae *Laminaria*	w:b = 20:1 t = 2 h T = 220°C	12 r 100%	23 – 185	--
Xu et al. (2020)	Sewage sludge from a municipal wastewater treatment plant	w:b = 1:1 -- T = 200°C	5 r 100%	--	6.94 – 8.28
		T = 230°C			7.06 – 8.27
		T = 260°C			7.44 – 11.25
Zhang et al. (2020)	50% water hyacinth and 50% sewage sludge	w:b = 10:1 t = 1 h T = 220°C	4 r --	30.58 to 49.39	11.25 – 19.00
Köchermann et al. (2018)	Municipal green waste – grass and shrub cuttings	w:b = 5.67:1 t = 5 h T = 180°C	11 r 89%	23 – 60	9 – 23
		T = 220°C	10 r 93%	27 – 92	10 – 39
Stemann, Putschew, & Ziegler (2013)	Dry poplar wood chips	w:b = 3:1 t = 4 h T = 220°C	4 r --	50 – 101	17.4 – 39.2
Xu (2020)	Pomegranate	w:b = 10:1 t = 4 h T = 220°C	4 r 50%	13.66 – 19.56	--
		T = 240°C		12.70 – 15.57	--

1: w:b – water to biomass ratio, t – time, T – temperature

2: r – recirculation; % of water requirement that is HTC liquor

6 MATERIALS AND METHODS

In this section, the feedstock material, equipment, experimental procedures, and analytical methods are described in detail.

6.1 Feedstock material

Primary sludge and biosludge were collected from the wastewater treatment plant of the UPM Kaukas pulp mill located in Lappeenranta, Finland. The sampling period of the sludges represented normal process operating conditions for the mill. The samples were stored in several polyethylene buckets in a freezer (-10 °C) prior to analysis to avoid or minimize biological, chemical, and physical changes that can occur between the time of collection and the experimental procedures.

6.2 HTC reactors

HTC of primary sludge and biosludge was performed in the laboratory facilities of Lappeenranta-Lahti University of Technology LUT in two different reactors. The reactor with a capacity of 1 L was used to evaluate properties of primary sludge and biosludge while 30- and 60-mL autoclave reactors were used for the biosludge recirculation test.

6.2.1 HTC 1 L reactor

HTC of primary sludge and biosludge was performed in a 1 L batch reactor designed and built at Lappeenranta-Lahti University of Technology LUT. The reactor, pictured in Figure 12, has a stainless-steel tube with a flange connection at the top and a screw cap at the bottom. A 10-kW electric heater coil heats the reactor tube, and the unit is covered by a layer of insulation as well as an outer steel sheet. The reactor is mounted on a frame and encased in a plexiglass safety box. Lower and upper thermocouples measure the temperature inside the reactor tube, and a third measures the outside surface. A proportional integral derivative controller maintains the temperature inside the reactor. Additionally, a pressure sensor and safety valve are installed for pressure measurements and safety. Thermocouples and the pressure sensor record data every 3 seconds.

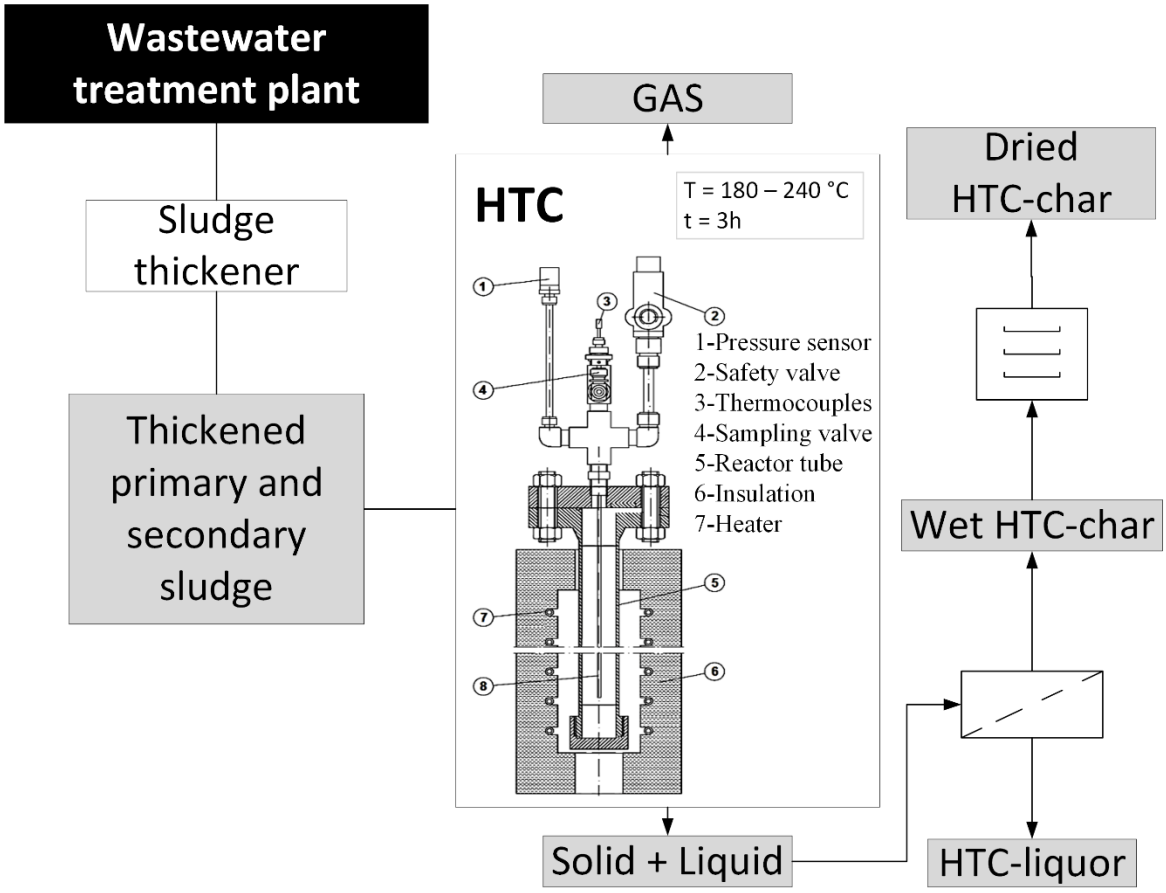

Figure 12. HTC 1 L reactor.

6.2.2 Hydrothermal autoclave reactors

HTC with recirculation was performed in Techinstro hydrothermal autoclave reactors with Teflon chambers. The hydrothermal reactor consists of a stainless-steel jacket and a Teflon chamber. As shown in Figures 13 and 14, the stainless-steel jacket has bottom and top gaskets as well as primary and secondary screw-type threaded caps. The Teflon chamber contains a vessel and a push-on cap. The hydrothermal reactors have a maximum operating temperature of ≤ 240°C, safe temperature of 200°C, working pressure of ≤ 3 MPa, and heating and cooling rate of ≤ 5°C / min (Techinstro, 2021).

Figure 13. Hydrothermal autoclave reactor.

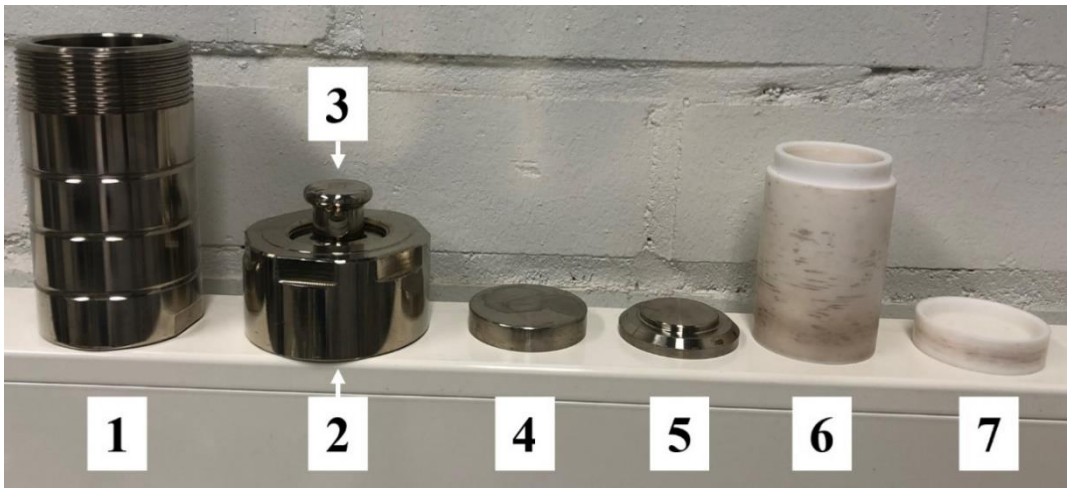

Figure 14. Hydrothermal autoclave reactor: 1) Stainless-steel jacket; 2) primary cap; 3) secondary cap; 4) top gasket; 5) bottom gasket; 6) Teflon vessel; 7) Teflon cap

6.3 Experimental procedure

In this work, two experimental conditions were analyzed, HTC of primary sludge and biosludge as well as HTC liquor recirculation of biosludge.

6.3.1 HTC of primary sludge and biosludge in 1L reactor

An 8:1 water-to-biomass ratio, approximately 50 g of biomass and 310 g of tap water, was tested. A steady residence time of three hours was used for reaction temperatures of 180, 200, 220, and 240°C. PSx refers to primary sludge treated at x°C, while BSx refers to

biosludge treated at x°C. After HTC, the solid-liquid slurry was released from the reactor tube. The primary sludge product was separated by vacuum filtration using VMR 600 qualitative filter paper (13 μm particle retention) inside a Büchner funnel. The liquid fraction, referred to as HTC liquor in this study, was collected in plastic vials and stored in a refrigerator at 4 ± 2°C. The biosludge product was separated in a similar way but instead of using vacuum, it was filtered overnight in a control chamber due to its slow filtration rate. Both primary sludge and biosludge solid fractions were dried overnight at 105 ± 5°C. The next day the hydrochar was collected, weighed, and stored in sealed plastic bags. The sample size was homogenized before characterization analysis. Additionally, untreated primary sludge and biosludge were dried – PSdried and BSdried – as well as filtered – PSraw and BSraw, respectively.

6.3.2 HTC recirculation of biosludge

In the second experimental condition, HTC recirculation was performed at a smaller scale. The focus was biosludge since in the first experimental condition, HTC was found to enhance biosludge more than primary sludge, and often in the pulp mills primary sludge is already incinerated. Three 30 mL and one 60 mL hydrothermal autoclave reactors were used. Before use biosludge was filtered with VMR 454 quantitative filter paper (12-15 μm particle retention) in a Büchner funnel. The same 8:1 water-to-biomass ratio was used. After adding the sample to the chamber, it was shaken by hand for 1 minute to ensure proper mixing. Next the chamber was placed inside the jacket and both primary and secondary caps were screwed on tightly. The autoclaves were placed in an oven at 160 ± 10°C for 4 hours – 1 hour to reach the reaction temperature and 3 to hold at the residence time. After heating, the autoclaves were removed from the oven and placed on a heat-resistance surface for 1 to 1.5 hours to cool. The contents were filtered as stated above. The liquid and solid fractions were stored in the same way as the first experimental condition. For following tests, in addition to fresh biosludge, a percentage of the previously collected HTC liquor was used in place of water. The labeling system is further explained in Table 10. The recirculation tests were performed at 160°C at dilutions of 60, 40, and 20%. An additional test was performed at 200 ± 10°C with 20% recirculation. 160°C was chosen because it is the lowest effective HTC temperature, while 200°C resulted in ideal properties in the first experimental condition and is used in industrial applications such as the Stora Enso paper mill.

Table 10. HTC recirculation labeling system.

Label	Explanation
BSx_y_0	HTC performed at x°C with 100% pure water and recirculated in BSx_y_1
BSx_y_1	HTC performed at x°C with y% BSx_y_0, 100 – y% pure water, and recirculated in BSx_y_2
BSx_y_2	HTC performed at x°C with y% BSx_y_2, 100 – y% pure water, etc.

x = temperature; y = dilution

6.4 Analytical methods

Feedstock, hydrochar, and liquid products were characterized using standard procedures. For the 1 L reactor samples, at least two measurements were taken for each temperature, and the average values were reported. For the autoclave reactors, only one measurement was taken for the solid characterization, so the values were compared to results from the first experimental condition and projected for better accuracy.

6.4.1 Solid characterization

Several techniques were carried out to characterize the solid fraction of HTC.

Mass yield

Mass yield of the solid after HTC was calculated according to Equation 1.

$$MY = 100 \times \frac{m_{hydrochar,dry}}{m_{sludge,dry}} \quad (1)$$

MY = mass yield [%]
m = mass [g]

Proximate analysis

The proximate analysis was performed to determine mass percentages of moisture, ash, volatiles, and fixed carbon of the samples. The hydrochar moisture content was measured according to standard DIN EN 14774-1 in the Shimadzu MOC-120H moisture balance. Ash content was determined using standard DIN EN 14775 at a maximum temperature of 550 ±

10°C and volatile content using standard DIN EN 15148. Ash, volatiles, and fixed carbon were calculated according to Equations 2 – 4.

$$A = 100 \times \frac{m_{out}}{m_{in}} \times \frac{100}{100-MC} \quad (2)$$

$$V = (100 \times \frac{m_{in} - m_{out}}{m_{in}} - MC) \times \frac{100}{100-MC} \quad (3)$$

$$FC = 100 - A - V \quad (4)$$

A = ash content [%]

m = mass [g]

MC = moisture content [%]

V = volatile matter [%]

FC = fixed carbon [%]

Ultimate analysis

The ultimate analysis was performed to determine the elemental composition of the samples. Carbon (C), hydrogen (H), and nitrogen (N) content were measured in the LECO CHN628 system and sulfur (S) content in the LECO 628S system using standards DIN EN 15407 and 15408, respectively. Oxygen (O) content was calculated according to Equation 5.

$$O = 100 - C - H - N - S - A \quad (5)$$

O = oxygen content [%]

C = carbon content [%]

H = hydrogen content [%]

N = nitrogen content [%]

S = sulfur content [%]

A = ash content [%]

Heating value

Hydrochar was densified in a pellet press and its HHV measured in the Parr 6400 automatic isoperibol calorimeter using standard DIN EN 14918. HHV_{dry}, LHV_{dry}, energy densification (ED), and energy yield (EY) were calculated according to Equations 6 – 9.

$$HHV_{dry} = HHV \times \frac{100}{100 - MC} \quad (6)$$

$$LHV_{dry} = \frac{(HHV_{dry} \times 238.85) - 600 \times \frac{9H}{100}}{238.85} \quad (7)$$

$$ED = \frac{HHV_{hydrochar,dry}}{HHV_{sludge,dry}} \quad (8)$$

$$EY = MY \times ED \quad (9)$$

HHV = higher heating value [MJ/kg]
MC = moisture content [%]
LHV = lower heating value [MJ/kg]
H = hydrogen content [%]
ED = energy densification [%]
EY = energy yield [%]
MY = mass yield [%]

For the HTC recirculation experiment, three correlations, Equations 10 – 12, were compared to calculate $HHV_{theoretical}$. $HHV_{theoretical\_1}$ is derived from the HTC of poplar, straw, and fresh grass, $HHV_{theoretical\_2}$ from over 219 sewage sludge samples, and $HHV_{theoretical\_3}$ from 250 various biomass residues (Kieseler, Neubauer, & Zobel 2013; Thipkhunthod et al., 2005; Nhuchhen & Salam, 2012). Equation 6 was used to find $HHV_{dry,\ theoretical}$.

$$HHV_{theoretical\_1} = 0.4108 \times FC + 0.1934 \times V - 0.0211 \times A \quad (10)$$

$$HHV_{theoretical\_2} = 0.28388 \times FC + 0.25575 \times V - 2.38638 \quad (11)$$

$$HHV_{theoretical\_3} = 19.288 + 0.0234 \times \frac{FC}{A} - 0.2135 \times \frac{V}{FC} - 1.9584 \times \frac{A}{V} \quad (12)$$

$HHV_{theoretical}$ = calculated higher heating value [MJ/kg]

FC = fixed carbon [%]

V = volatile matter [%]

A = ash content [%]

Fourier-transform infrared spectroscopy (FTIR)

Fourier-transform infrared spectroscopy (FTIR) was performed in a PerkinElmer Frontier FT-IR Spectrometer to determine the functional groups present in the sample. A universal diamond crystal attenuated total reflection module was used between 400 and 4000 cm^{-1} with a resolution of 4 cm^{-1}.

Inductively coupled plasma optical emission spectrometry (ICP-OES)

Inductively coupled plasma optical emission spectrometry (ICP-OES) was used to determine trace elemental concentrations of aluminum (Al), silver (Ag), cadmium (Cd), cobalt (Co), chromium (Cr), copper (Cu), iron (Fe), potassium (K), magnesium (Mg), manganese (Mn), molybdenum (Mo), sodium (Na), nickel (Ni), phosphorus (P), lead (Pb), silicon (Si), uranium (U), vanadium, (V), and zinc (Zn) in the Thermo Fischer Scientific iCAP 6000 ICP emission spectrometer. Solid samples were centrifuged for 10 to 20 minutes at 5000 rpm, then digested for 20 minutes under the addition of HCl (hydrochloric acid) and HNO_3 (nitric acid).

Thermogravimetric analysis (TGA)

Thermogravimetric analysis (TGA) was performed with the Netzsch-Gerätebau Jupiter 449C simultaneous thermal analyzer. 10 mg of solid was placed in the Al_2O_3 (aluminum oxide) sample holder. The furnace was sealed and purged with high purity (99.9995%) nitrogen to remove air. Then the sample was heated from room temperature to 900°C at a rate of 20 K/min. Two different gas atmospheres were tested (high purity nitrogen for pyrolysis and compressed air for combustion) using a constant gas flow rate of 250 mL/min.

Scanning electron microscopy (SEM)

A Hitachi SU3500 microscope was utilized for scanning electron microscopy (SEM) to examine the morphology of the samples, using a backscattered electron (BSE) detector to take the images.

X-ray diffraction (XRD)

The Bruker D8 ADVANCE X-ray powder diffractometer was used for X-ray diffraction (XRD) to determine the degree of crystallinity. Samples were analyzed with Cu Kα monochromatic radiation and θ-2θ geometry. X-ray diffractograms were produced in the 10–60° (2θ) range with step length of 0.0204° and step-counting time of 0.725 s. Two different methods were used to calculate the crystallinity index, shown in Equations 13 and 14. For Equation 14, OriginPro software was used to find peaks and area from the output data.

$$CI_1 = 100 \times \frac{I_{002} - I_{am}}{I_{002}} \quad (13)$$

$$CI_2 = \frac{Area_{crystalline}}{Area_{crystalline} + Area_{amorphous}} \quad (14)$$

CI = crystallinity index [%]
I_{002} = diffraction intensity at 2θ = 22° [counts]
I_{am} = diffraction intensity at 2θ = 18° [counts]
Area = area under peaks [°counts]

6.4.2 Liquid characterization

The following analytical methods were performed to characterize the HTC liquor.

pH

After filtration pH was measured at least three times with a Metrohm 744 pH meter.

NVR, inorganic, and organic content

Approximately 3 mL of each sample's HTC liquor was pipetted into pre-weighed crucibles. They were dried overnight at 105 ± 5°C and weighed again to find the non-volatile residue (NVR) content. The remaining organic content was burned off at 550 ± 10°C for one hour, cooled, and weighed to determine the inorganic content. NVR, inorganic, and organic content were calculated according to Equations 15 – 20.

$$NVR_g = m_{out,105°C} = Inorganic_g + Organic_g \quad (15)$$

$$NVR_{\frac{g}{kg}} = \frac{NVR_g}{0.001 \times m_{in,105°C}} \quad (16)$$

$$Inorganic_g = m_{out,550°C} \quad (17)$$

$$Inorganic_{\frac{g}{kg}} = \frac{Inorganic_g}{0.001 \times m_{in,105°C}} \quad (18)$$

$$Organic_g = NVR_g - Inorganic_g \quad (19)$$

$$Organic_{\frac{g}{kg}} = \frac{Organic_g}{0.001 \times m_{in,105°C}} \quad (20)$$

$NVR_{g,\,g/kg}$ = non-volatile residue content [g, g/kg]

m = mass of liquid sample [g]

$Inorganic_{g,\,g/kg}$ = inorganic content [g, g/kg]

$Organic_{g,\,g/kg}$ = organic content [g, g/kg]

TC, TOC, and IC

Total carbon (TC), total organic carbon (TOC), and inorganic carbon (IC) were measured in the Shimadzu TOC-L CPN Total Organic Carbon Analyzer. Dilutions of 10 – 100 mg/L were used according to standard procedure EN 1484-H3.

COD

The chemical oxygen demand (COD) test was prepared by adding liquid sample as well as potassium dichromate, sulfuric acid, and mercury sulfate to Hach Lange test cuvettes suitable for a COD range of 20 – 1500 mg/L. The test cuvettes were heated for two hours at 150°C, and then COD values were determined with the Hach Model DR/2010 Spectrophotometer at a wavelength of 620 nm.

Inductively coupled plasma optical emission spectrometry (ICP-OES)

The ICP-OES method applied for the solid samples was also used to find the trace elemental concentrations of the HTC liquor.

7 RESULTS AND DISCUSSION

In this section, results are presented, analyzed, and compared with literature data.

7.1 HTC of primary sludge and biosludge

Solid and liquid properties were measured for untreated and treated primary sludge and biosludge.

7.1.1 Solid characterization

Figure 15 shows the primary sludge and biosludge hydrochar as well as dried samples. The primary sludge hydrochar is light, fibrous, and fluffy due to the primary sludge's high fiber content. PS240 is darker and more likely to crumble than the others. As the reaction temperature increased, the biosludge hydrochar lost its charcoal consistency and was replaced by a powder-like consistency.

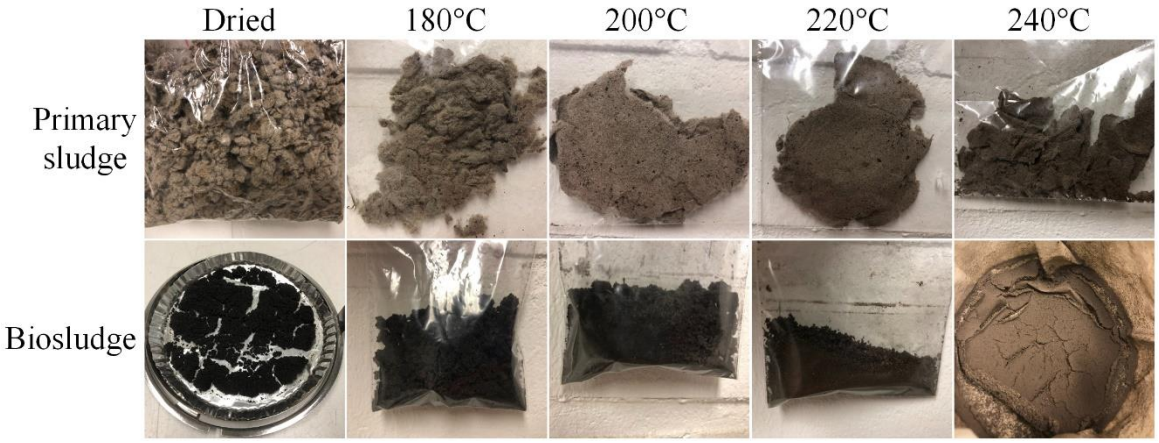

Figure 15. Dried sludge and hydrochar.

Table 11 shows the main characterization parameters of the solid fraction including the proximate and ultimate analyses as well as heating value.

Table 11. Primary sludge and biosludge solid characterization.

	Primary sludge						Biosludge					
°C	Untreated	Dried	180	200	220	240	Untreated	Dried	180	200	220	240
Proximate analysis (% wt, dry)												
MY	--	--	50.27	62.65	55.35	29.21	--	--	79.35	74.97	63.93	57.10
MC	96.80	5.14	7.10	6.81	6.42	5.82	92.18	3.23	5.65	6.39	4.94	3.20
A	9.45	8.03	5.88	6.12	6.45	9.49	20.99	16.59	17.18	18.84	18.90	20.87
V	93.42	78.13	88.40	85.71	86.04	81.30	69.16	61.98	63.33	56.75	55.21	52.97
FC	--	13.89	5.97	8.32	8.22	9.44	9.85	22.30	19.96	25.23	26.70	26.82
Ultimate analysis (% wt, dry ash-free basis)												
C	--	40.87	43.68	43.23	44.43	44.13	--	44.76	46.10	46.59	52.66	52.57
H	--	6.30	6.31	6.25	6.28	6.05	--	5.80	5.66	5.91	5.97	5.70
N	--	0.67	0.43	0.37	0.26	0.28	--	4.36	4.14	4.01	2.88	2.99
S	--	0.42	0.23	0.20	0.20	0.24	--	2.30	2.27	2.22	2.27	2.28
O	--	43.71	43.47	43.82	42.38	39.80	--	26.20	24.63	22.43	17.32	15.59
H/C	--	1.84	1.75	1.72	1.69	1.62	--	1.55	1.50	1.51	1.35	1.29
O/C	--	0.80	0.76	0.75	0.72	0.67	--	0.44	0.40	0.36	0.25	0.22
Heating value (MJ/kg, dry)												
HHV	--	17.50	18.58	18.57	18.70	18.78	--	19.78	21.01	24.45	24.47	24.78
LHV	--	16.07	17.14	17.15	17.28	17.41	--	18.47	19.73	23.11	23.12	23.49
ED (--)	--	--	1.06	1.06	1.07	1.07	--	--	1.06	1.24	1.24	1.25
EY (%)	--	--	53.36	66.48	59.14	31.34	--	--	84.27	92.65	79.08	71.52

MY: mass yield; MC: moisture content; A: ash content; V: volatile matter; FC: fixed carbon; HHV: higher heating value; LHV: lower heating value; ED: energy densification; EY: energy yield

Mass yield

The mass yield decreased for both primary sludge and biosludge hydrochar as the reaction temperature increased. This is due to more severe elimination and dehydration processes by which volatiles are released into the liquid phase at a higher rate. Additionally, gases and lighter organic compounds formed, which both reduced the mass yield and increased the hydrochar porosity (Salimi et al., 2017). The biosludge mass yield is between 57 and 80%, which is higher than that of primary sludge between 29 and 51%.

Proximate analysis

Figure 16 depicts the proximate analysis as well as heating value behavior according to type of sludge and reaction temperature. Ash and volatile content decreased after HTC compared to wet, untreated sludge. The sludge lost light compounds upon drying, which is why dried sludge resulted in lower volatiles than the treatment at 180°C. Furthermore, ash content generally increased with reaction temperature while volatile matter decreased, with biosludge having lower volatiles but higher ashes and fixed carbon than primary sludge. The high volatile matter and low fixed carbon of primary sludge leads to faster burning (Rodrigues et al., 2021), one reason why primary sludge is combusted in pulp mills. Ash increases with temperature because HTC breaks down organic components in the biomass and releases them into the liquor, while inorganic compounds are simultaneously concentrated in the hydrochar (Saha et al., 2019). Additionally, the high ash content of biosludge is attributed to its high concentration of inorganic compounds, hindering combustion efficiency. Specifically, alkali metals, alkaline earth metals, and Al can cause boiler fouling, slagging, and corrosion, while heavy metals may emit noxious fumes (Zhang et al., 2020). However, ash can be beneficial for providing nutrients in soil application.

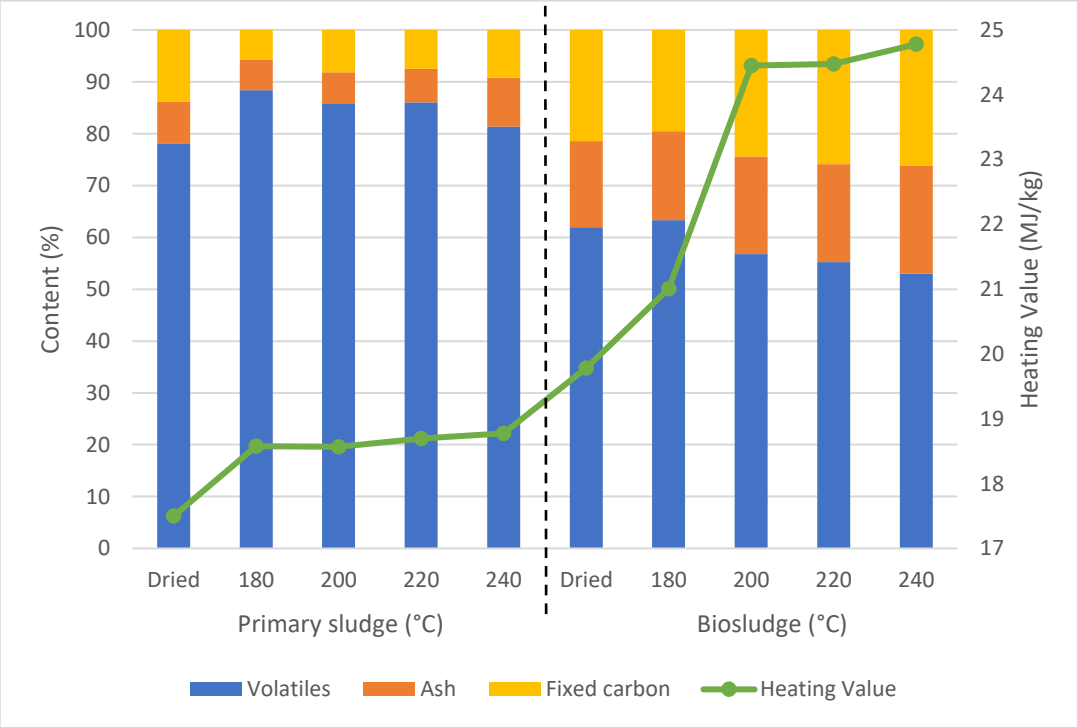

Figure 16. Proximate analysis and heating value for primary sludge and biosludge.

Ultimate analysis

Primary sludge contains relatively equal amounts of C and O, while biosludge contains considerably higher C. Biosludge also contains more H, N, and S than primary sludge. Carbon increased with temperature while oxygen decreased, which is more notable for biosludge. These trends are portrayed in the Van Krevelen diagram in Figure 17 along with various fuels for comparison. A sample closer to the origin, such as anthracite, is a higher quality fuel, whereas moving farther away from the origin, like cellulose, indicates a lower quality fuel (Saha et al., 2019). Primary sludge H/C and O/C atomic ratios decreased from 1.84 to 1.62 and 0.80 to 0.67, respectively, between PSdried and 240. Biosludge H/C and O/C atomic ratios both began lower, with O/C nearly half that of primary sludge. The H/C and O/C ratios dropped from 1.55 to 1.29 and 0.44 to 0.22, respectively, between BSdried and 240. According to Salimi et al. (2017) and the present study, HTC is more impacted by decarboxylation and dehydration and only negligibly by demethanation, thus the former two reactions are essential pathways for HTC. This can be seen as the treated samples slid down both axes but not in the positive direction for O/C. Biosludge is plotted closer to the energy dense fuels such as coal, indicating that biosludge is a better fuel than primary sludge. This is also confirmed by biosludge's higher heating value presented in the next section.

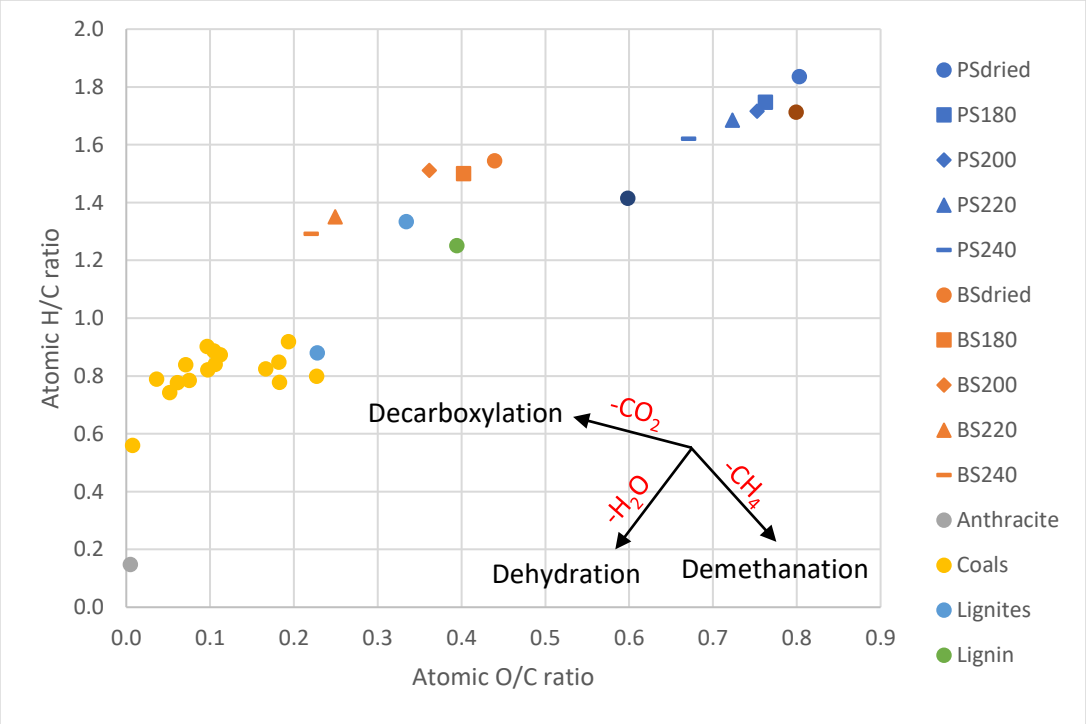

Figure 17. Van Krevelen diagram (Van Loo & Koppejan, 2008).

Heating value

HHV increased from 19.78 to 24.78 MJ/kg for BSdried and 240, respectively. However, primary sludge HHV only increased from 17.50 to 18.78 MJ/kg, which is also 1 MJ/kg less than BSdried. Energy densification is 1.06 or 1.07 for all primary sludge hydrochars and biosludge hydrochars at 180°C. The subsequent biosludge hydrochars have higher energy densification at 1.24 and 1.25. Energy yield generally decreased with higher HTC temperatures but increased at 200°C, perhaps indicating that this treatment is the most ideal balance of mass yield and energy densification. On the other hand, biosludge has 1.34 to 2.28 times higher energy yields due to larger mass yields and energy densifications. In terms of the change in heating value, HTC seemed to have a much greater effect on biosludge than primary sludge.

Fourier-transform infrared spectroscopy (FTIR)

FTIR of PS and BSdried, 180, and 240 are shown in Figure 18. The peaks are labeled with their associated functional groups including kaolinite, aromatics C=C, O-H, C-H, C-O, C-O-C, and C=O. Primary sludge and biosludge have 11 and 10 peaks, respectively. They display similar peaks at the beginning but begin to differ between 600 and 1800 cm^{-1}. Additionally, each type of sludge contains similar peaks, but the higher HTC temperatures have bigger peaks, meaning the samples contain a larger content of these functional groups. In PS240, peaks at 1708 and 1602 cm^{-1} did not appear in the other samples, while the small peaks around 900 cm^{-1} in PSdried and PS180 did not register in PS240. Biosludge experienced more peak shifting, up to 55 cm^{-1}, while primary sludge only shifted a maximum of 8 cm^{-1} per peak. Table 18 in Appendix 2 details these peaks.

According to Méndez et al. (2009) the characteristic peaks of cellulose are located 3600 to 3200, 2900 to 2800, 1630, 1430, 1367, 1315, 1270, 1160, 1110, 1055, 1026, and 878 cm^{-1}. Primary sludge matches this fairly well due to its high content of cellulose. Primary sludge peaks around 1430 and 900 cm^{-1} represent calcium carbonate ($CaCO_3$) and biosludge peaks around 3680, 1015, and 865 cm^{-1} signify kaolinite ($Al_2Si_2O_5(OH)_4$), both which are common additives in pulp and paper mill sludge (Niinipuu et al., 2020; Mäkelä, Benavente, & Fullana, 2015).

According to Wang, Chen, & Jang (2020), hydrochar peaks decreased around 3300 and 1600 cm^{-1} due to dehydration and decarboxylation, respectively, because of HTC, which intensified with increased temperature. However, in the present study hydrochar at 240°C has the largest peaks and dried sludge has the smallest. Peaks around 3300, 2900, and 1600 cm^{-1} are associated with O-H vibration in the hydroxyl group, C-H stretching, and C=O stretching in the carboxylic group, the latter of which is caused by the oxidation of cellulose fibers. The peaks between 1500 and 1700 cm^{-1} are attributed to the aromatic structure of C=C. Additionally, primary sludge peaks surrounding 1100 are C-O-C, indicating hemicellulose or degraded cellulose, while the band at 1030 is C-O stretching of the remaining cellulose and hemicellulose in the cell walls (Méndez et al., 2009; Salimi et al., 2017).

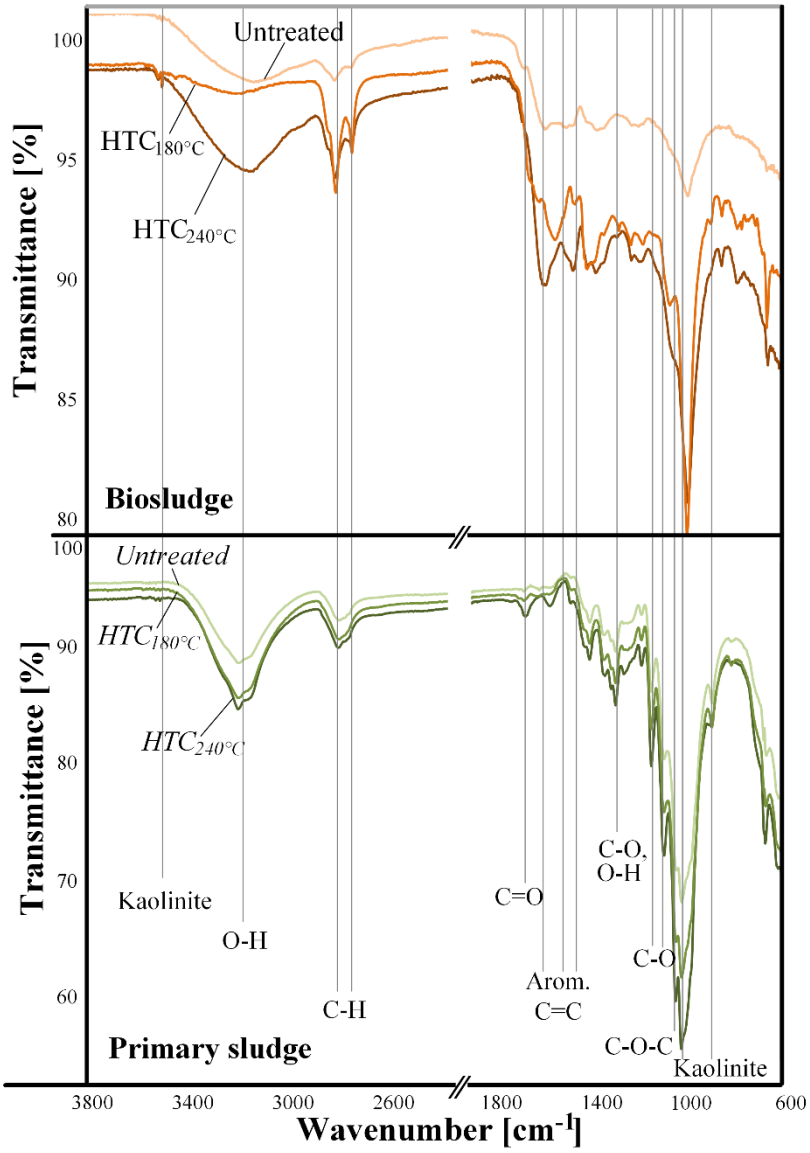

Figure 18. FTIR of primary sludge and biosludge.

Inductively coupled plasma optical emission spectrometry (ICP-OES)

Biosludge has a significantly higher trace elemental concentration than primary sludge, as seen in Figure 19. Concentration reduced slightly in BS180 and 200 but then increased again. Particularly, biosludge is high in Al, P, and Na. In biosludge, Al continued to increase as the HTC temperature increased, but the concentration remained relatively stable for different primary sludge treatments. Al-based chemicals are utilized as property-enhancing filler for board production as well as a flocculating agent in the wastewater treatment process (Pöykiö, Watkins, & Dahl, 2018; Mäkelä et al., 2018). For other elements in biosludge such as Cr, Ni, and Mo, HTC drastically reduced the concentration compared to the dried sample,

though increasing temperatures had varying effects. Primary sludge did not undergo this same reduction.

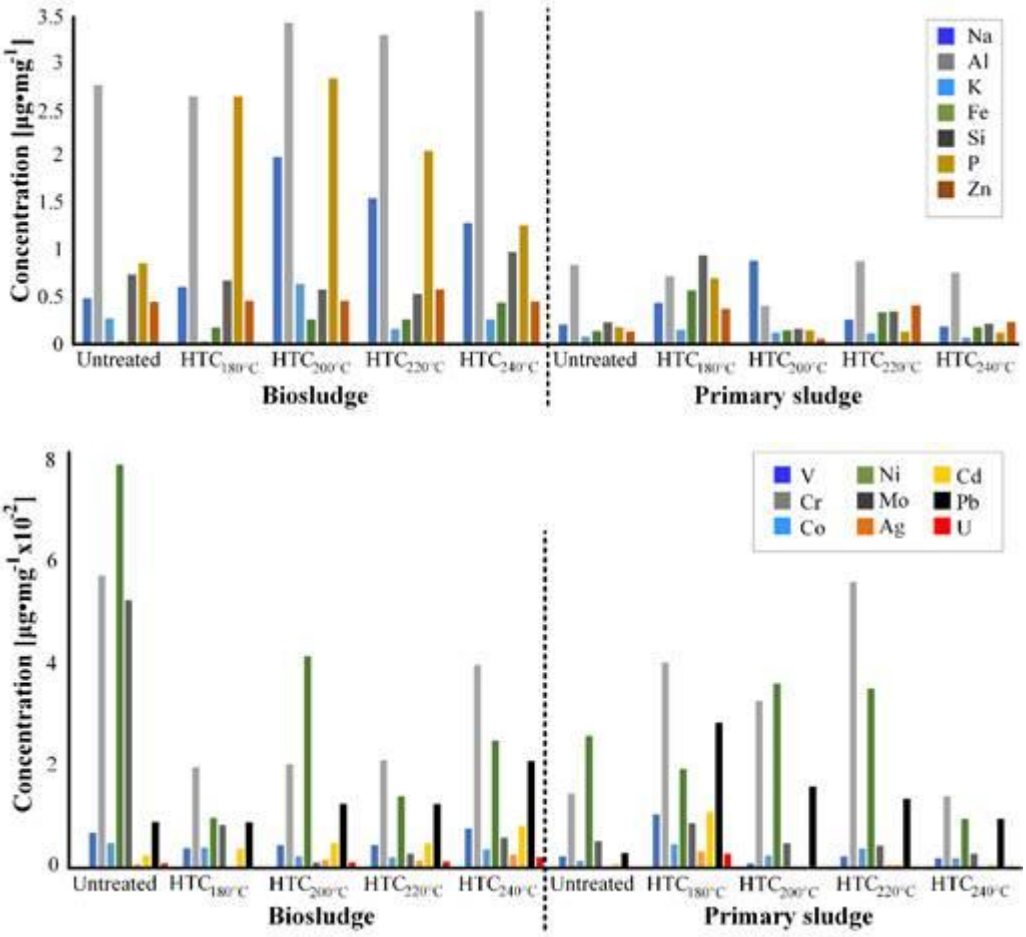

Figure 19. Trace elemental concentration of dried sludge and hydrochar.

The review by Huang & Yuan (2016) found that total heavy metal content of sewage sludge hydrochar is higher than that of raw sewage sludge, which is consistent with this study. This is due to decomposition and transformation of organic compounds. Furthermore, Shi et al. (2013) observed that hydrochar heavy metal concentration increased with HTC reaction temperature, which is partially consistent with this study. Higher temperatures allow for the immobilization of metals in the sludge, transforming the metals from weakly to stably bounded as well as decreasing the leachable fraction and toxicity. BSdried has a total trace elemental concentration of 5833 mg/kg, which peaked at 10211 mg/kg for BS200 and reduces back down to 8260 mg/kg for BS240. PSdried started at a concentration 4000 mg/kg

lower than BSdried, but the HTC treatments fluctuated in no order, from a peak of 3912 mg/kg for PS180 to a trough of 1763 mg/kg for PS240.

Moreover, if hydrochar is used for soil amendment, it must follow regional guidelines. In the EU, hydrochar could be used as an organic fertilizer or soil improver. An organic soil improver contains material of 95% biological origin and functions not to add nutrients, like a fertilizer, but to maintain, improve, or protect the properties, structure, or biological activity of the soil (The European Parliament and the Council of the European Union, 2019). Table 12 presents trace elemental concentrations for this study, pulp mill sludge from literature, and EU metal limits for organic soil amendment.

Table 12. Pulp mill sludge trace elemental concentrations and EU soil limits.

	Present study				**Pöykiö, Watkins, & Dahl (2018)**		**Pöykiö et al. (2014)**	**Eskandari et al. (2019)**	**EU organic soil amendment metal limits**	
	Primary sludge		**Biosludge**		**Primary sludge**	**Biosludge**	**Biosludge**	**Biosludge**		
mg/kg	**Dried**	**240°C**	**Dried**	**240°C**	**Dried**	**Dried**	**Dried**	**200°C**	**Fertilizer**	**Soil Improver**
Na	210	187	489	1292	4000	42600	6490	810	--	--
Al	845	758	2762	3553	1910	8940	1850	--	--	--
K	81	71	276	263	< 200	2490	3260	1340	--	--
Fe	138	181	34	446	1930	6280	38700	--	--	--
Si	232	214	744	982	--	--	--	--	--	--
P	181	119	863	1268	320	5660	6260	2770	--	--
Zn	135	234	448	456	110	490	250	430	800	800
V	2.37	2.00	7.11	7.88	--	--	3.50	--	--	--
Cr	14.79	14.26	57.99	40.37	19.00	49.00	9.10	40.00	2.00	2.00
Co	1.57	2.01	5.07	3.74	< 1.00	2.80	4.70	--	--	--
Ni	26.21	9.84	80.86	25.34	8.60	32.00	14.00	20.00	50.00	50.00
Mo	5.42	2.89	53.11	6.12	< 1.00	4.70	2.20	--	--	--
Ag	0.27	0.24	0.85	2.76	--	--	--	--	--	--
Cd	0.81	0.72	2.60	8.48	0.50	4.80	1.40	10.00	1.50	2.00
Pb	3.04	9.84	9.22	21.34	< 3.00	6.00	< 3.00	20.00	120.00	120.00
U	0.33	0.29	1.04	2.24	--	--	--	--	--	--

(Pöykiö, Watkins, & Dahl, 2018; Pöykiö et al., 2014; Eskandari et al., 2019; The European Parliament and the Council of the European Union, 2019)

Primary sludge and biosludge fall well under the limits for Zn and Pb. However, only primary sludge meets the limits for Ni and Cd, while neither primary nor biosludge would

be permitted due to Cr. One benefit of HTC is that it reduces biosludge Ni to an acceptable concentration, though HTC also unfortunately increases Cd from nearly within the range to over four times in excess.

Thermogravimetric analysis (TGA)

Figure 20 presents the TGA curves of primary sludge and biosludge, which differ due to the atmosphere.

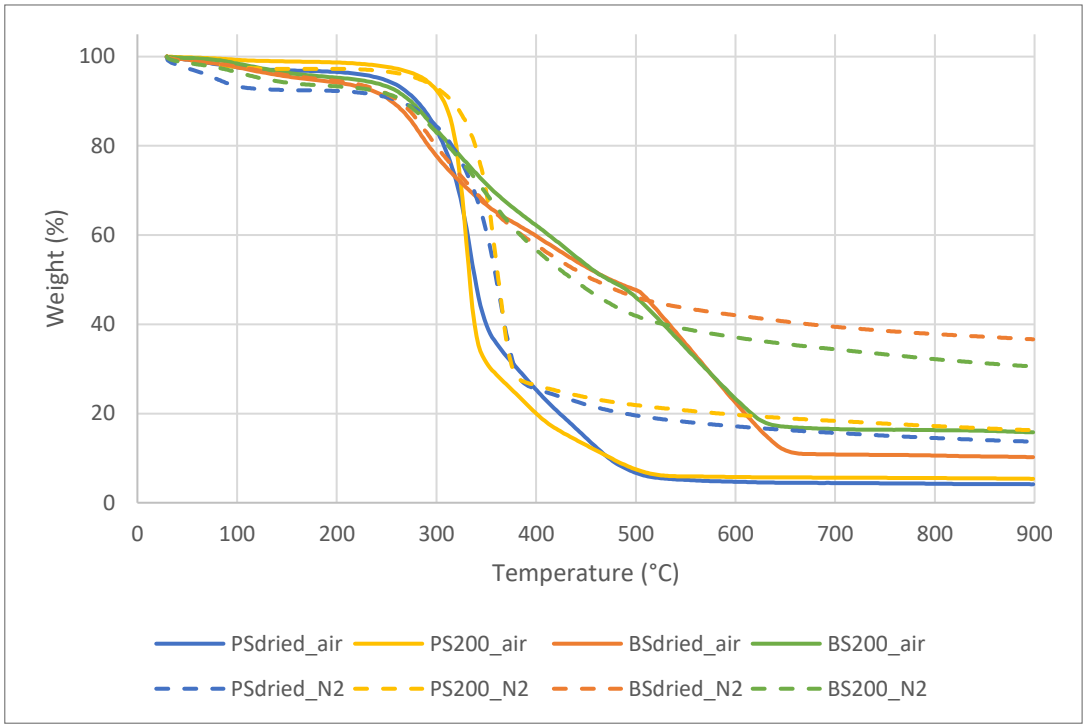

Figure 20. TGA of primary sludge and biosludge.

In the presence of nitrogen gas, dehydration, fast devolatilization, and carbonization occur. Between approximately 30 and 120°C, water in the sample vaporized, followed by most of the volatiles being released from 200 to 400°C, and further volatile degradation between 450 and 750°C. In air, however, carbonization is replaced with combustion in which char formed in the previous stage is burned and converted into CO_2 and H_2O (Ma et al. 2018; Tsai et al., 2009). Thermal events of biosludge during combustion can be found in Table 13.

Table 13. Thermal events in the combustion of biosludge (Zheng & Koziński, 2000).

Temperature range (°C)	Weight loss (%)	Possible processes
25–130	0–5	Vaporization of moisture
240–450	45–80	Volatilization, pyrolysis and initial burning of volatile compounds
400–600	0–5	Char formation
600–700	0–3	CaCO3 decomposition, char oxidation
800–1100	0–1	Metals reduction, volatilization of cadmium, copper, lead, nickel and zinc compounds

The derivative thermogravimetric (DTG) curves in Figure 21 show that primary sludge, both in nitrogen and air, has one main peak of weight loss. In nitrogen, PSdried and 200 lose 55% and 48% of their weight, respectively. The peak of PS200 occurs at 361°C, which is 3°C cooler than PSdried. This correlates with Rodrigues et al. (2021) in which primary sludge lost most of its weight between 225 and 375°C due to the thermal degradation of hemicellulose and cellulose. In air, primary sludge continued to combust rapidly until 500°C, causing a weight loss of approximately 10% more than in nitrogen. There is also higher weight loss at the peak in air, less than 1% higher for PSdried but over 10% higher for PS200. This is due to the accelerated devolatilization caused by oxygen combusting with volatiles and char (Ma et al. 2018). Similar to nitrogen, the PS200 peak in air occurs 4°C before the PSdried peak. However, the peaks occur about 30°C less for both samples, as observed by Amutio et al. (2012). In both atmospheres, PSdried has a lower final weight percentage, or a higher overall weight loss, than PS200.

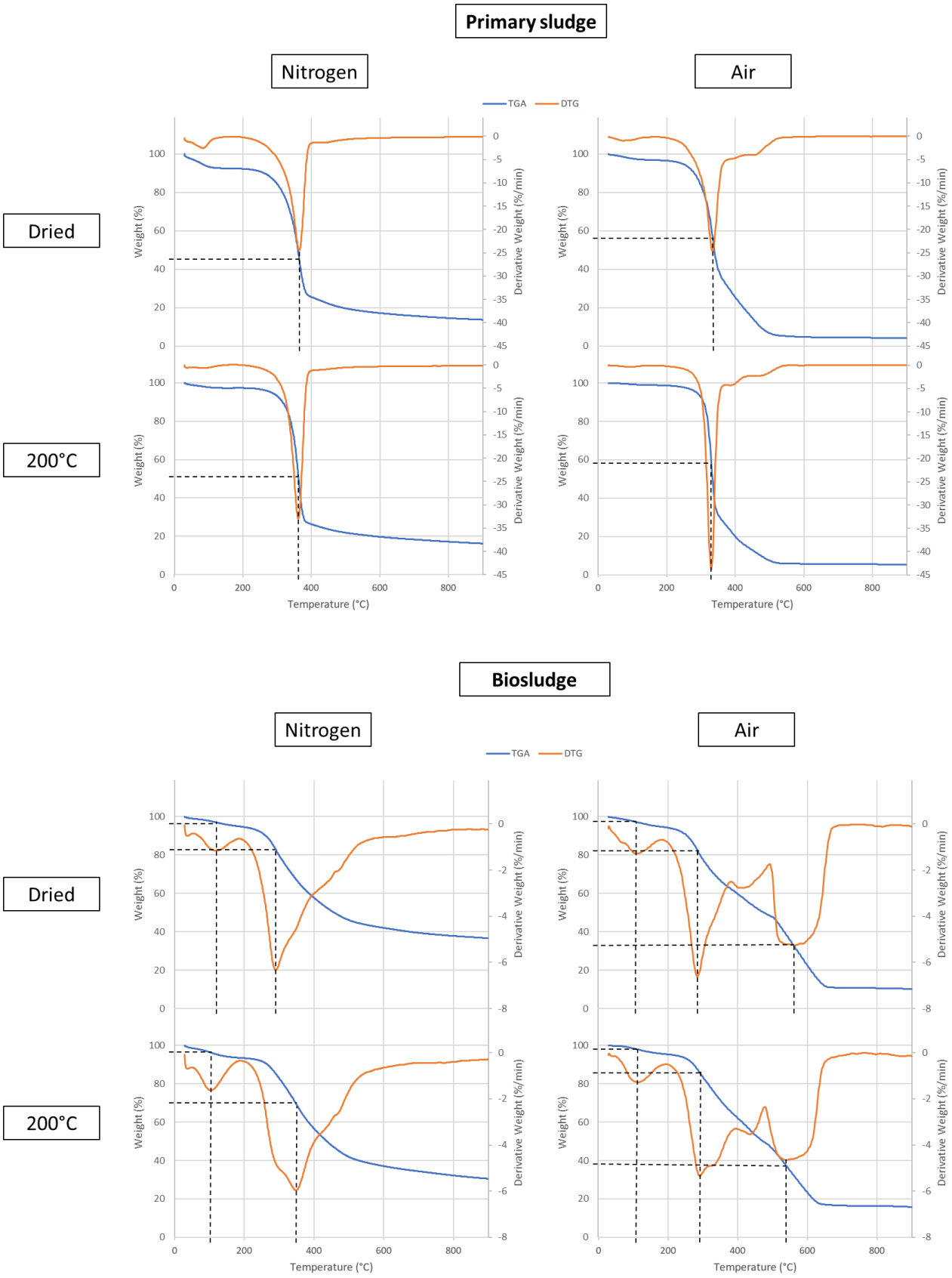

Figure 21. TGA and DTG curves of primary sludge and biosludge.

Biosludge has two peaks in nitrogen and three peaks in air. The biosludge curves are not as steep as primary sludge and less weight is lost since higher cellulosic content leads to higher biomass reactivity (Ghetti, Ricca, & Angelini, 1996). Zheng & Koziński (2000) observed similar peaks between 98 and 130°C as well as 130 and 400° caused by moisture evaporation and volatilization, respectively. The third peak in air is wide, almost a horizontal line between 500 and 600°C. This could be attributed to char formation as well as oxidation. Once again, air leads to a greater weight loss, 26% more for BSdried and 15% more for BS200, which is a 9% difference compared to only 1% with primary sludge. Additionally, BS200 does not follow the primary sludge trend in which the treated sample has an overall smaller weight loss. The weight loss is higher for nitrogen but lower for air. These results are another confirmation that HTC has a greater impact on biosludge than primary sludge.

Scanning electron microscopy (SEM)

BSE images of primary sludge and biosludge are pictured in Figures 22 and 23 with magnifications of 1 mm, 200 µm, and 50 µm. Dried, 180 °C, and 240°C were chosen to show the change between untreated samples as well as those treated at lower and higher temperatures. Primary sludge features long, homogeneous fibers, whereas the main structures of biosludge are amorphous particles. After HTC, the fibers and particles decreased in size, which is especially apparent in PS240 compared to PS180. These observations are also portrayed in Niinipuu et al. (2020). Due to this degradation, the mass yields decreased 1.31% between PS180 and 240 and 3.31% between BS180 and 240. In the 50 µm magnification, it is easier to see how the structures are cracked and damaged. This looks like fraying of the fibers in primary sludge and holes forming in the biosludge particles.

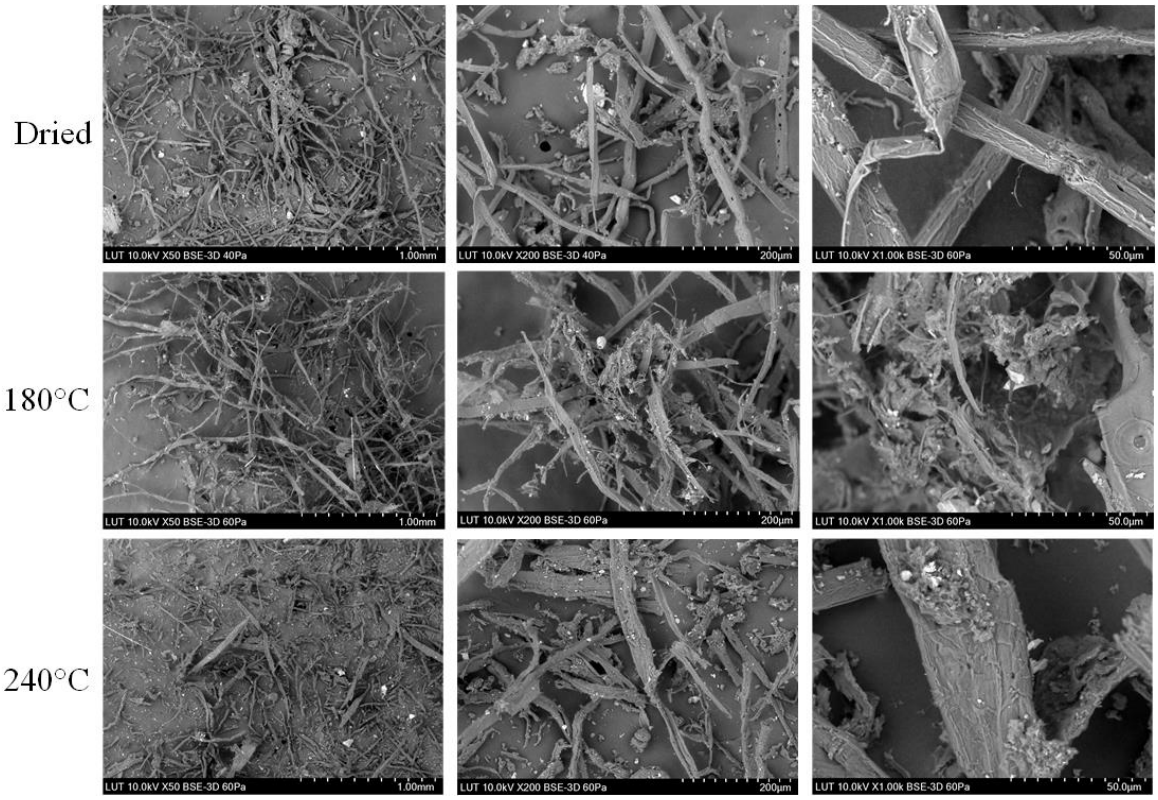

Figure 22. BSE images of PSdried, 180, and 240.

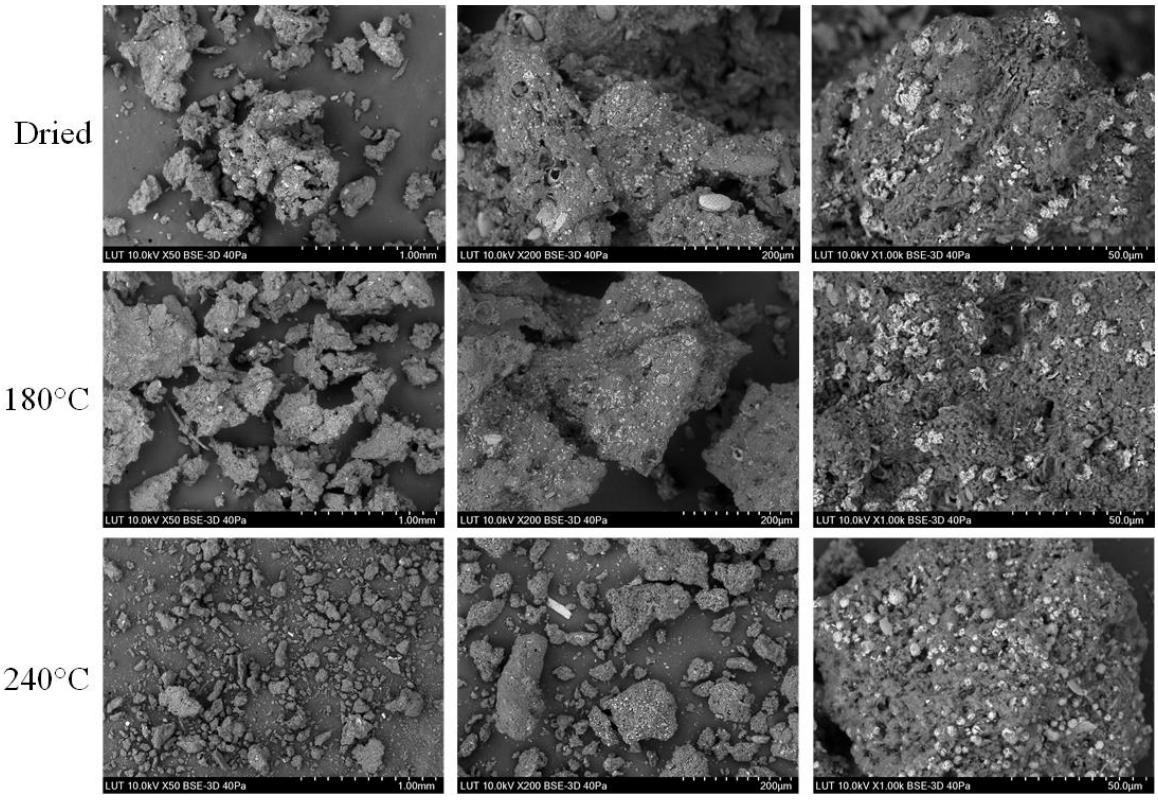

Figure 23. BSE images of BSdried, 180, and 240.

Two distinct features of biosludge can be seen in Figure 24. The shiny, white particles are inorganic material or contaminants. These are abundant since biosludge has a much higher concentration of trace elements than primary sludge. The patterned ovals are identified as *Euglypha*, microorganisms present in the wastewater treatment degradation stage.

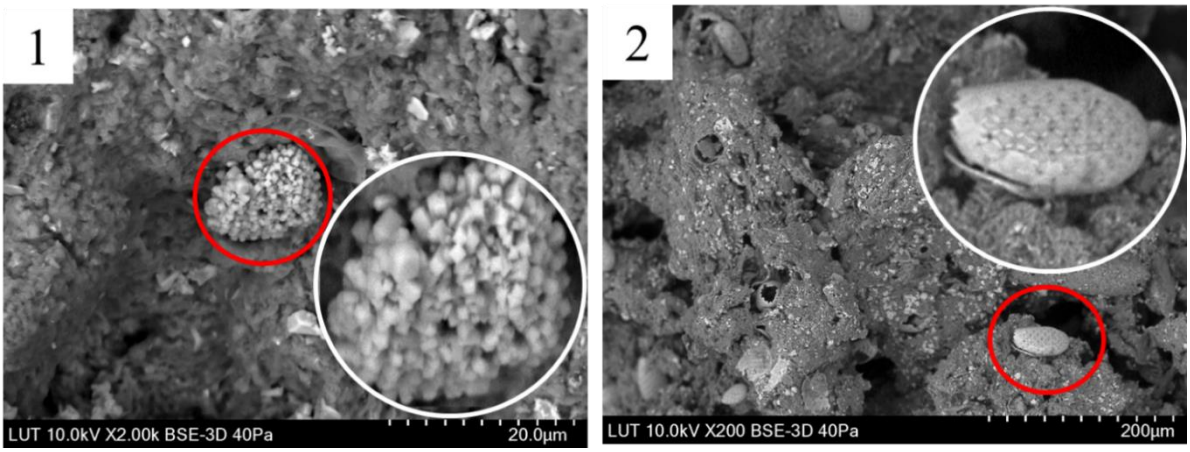

Figure 24. Biosludge features: 1) inorganic material in BS180; 2) *Euglypha* in BSdried
Note: The white circle is an enlargement of the red circle.

Figure 34 in Appendix 3 displays SEM mapping of BSdried in which different colors represent different elements including C, O, Na, Mg, Al, Si, P, S, Cl, K, Ca, Ti, Mn, and Fe.

X-ray diffraction (XRD)

The XRD graphs, presented in Figure 25, are similar for dried and 200°C treated samples. PSdried has large peaks at 16.18 and 22.55°, with a smaller peak at 34.77°, while PS200 has peaks at 16.40, 22.61, and 34.79°, all slightly shifted to the right on the 2θ axis. These peaks match the characteristic peaks for cellulose at 15.7, 22.6, and 35.19°, corresponding to lattice planes 110, 200, and 004, respectively (Trilokesh & Uppuluri, 2019). There is also a smaller peak at about 28.6°. This is likely calcium carbonate, which has a characteristic peak at 29.4° at lattice plane 104 (Chong, Chia, & Zakaria, 2014).

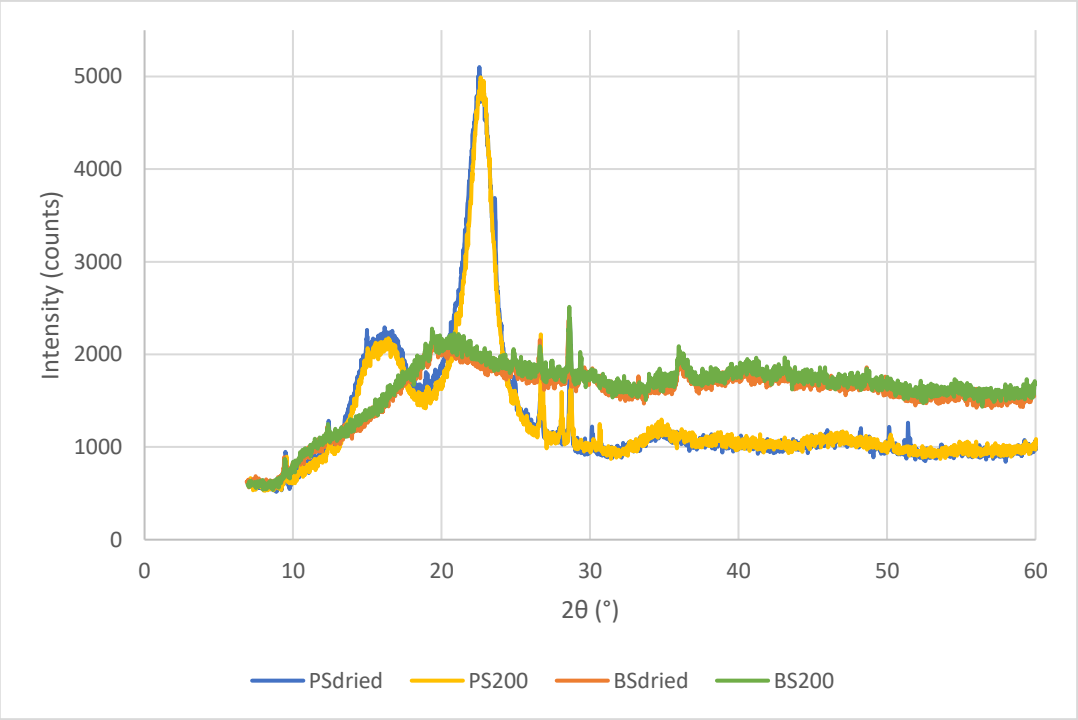

Figure 25. XRD of primary sludge and biosludge.

The crystallinity of primary sludge does not change significantly after HTC as expected. The first calculation method results in crystallinity indexes of 60.07 and 60.28% for PSdried and 200. Based on the second method with areas found in OriginPro, the crystallinity indexes reduce from 56.46 to 52.28%. Presumably the second method is more accurate since it considers all the peaks instead of just the most intense peak like in the first calculation.

Zhang et al. (2015) observed the disappearance of peaks at 16 and 22.7° with the HTC of corn cob residuals at 250°C. This is attributed to the decomposition of cellulose and destruction of crystalline structure into amorphous components. Kang et al. (2012) performed HTC of cellulose at 245°C, and also measured the absence of a crystalline peak at 22.7°. Conversely, Huang et al. (2021) noted that eucalyptus hydrochar peaks remained the same for treatments of 200 and 220°C but temperatures between 240 and 280°C resulted in the gradual flattening of the peaks at 16, 22, and 35°. Based on these findings, the XRD peaks of PS240 may also reduce in intensity due to the increased temperature.

Like primary sludge, both biosludge samples have similar peaks. However, biosludge does not contain any large peaks, indicating that it is largely amorphous (Baccile et al., 2013). A

few small peaks are observed between 9 and 13, 19 and 20, as well as 24 and 35°, which relatively line up with the small peaks in the primary sludge. Calcium carbonate also appears at a peak of 28.6°. Kogbara et al. (2020) showed a similar XRD analysis for wastewater treatment plant biosludge – the plot is relatively flat and there are few peaks. The biosludge crystallinity index calculation methods resulted in more varied numbers than primary sludge. The indexes for BSdried and 200 are 11.72 and 10.42%, respectively, for the first method but 48.45 and 48.42%, respectively, for the second method.

7.1.2 Liquid characterization

Figure 26 shows the primary sludge and biosludge raw filtrate and HTC liquor fraction. All the primary sludge samples are a similar shade of brown, while biosludge samples vary in color, ranging from light yellow to dark brown.

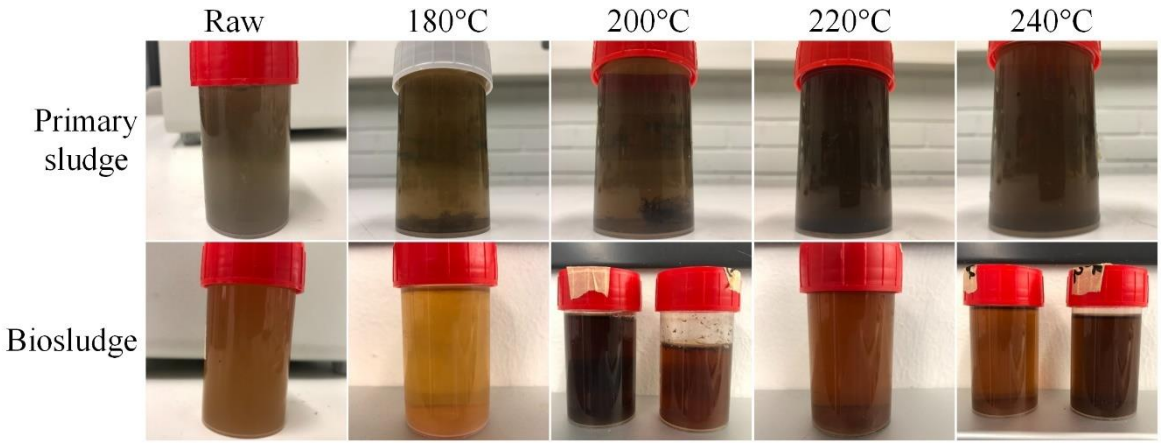

Figure 26. Raw filtrate and HTC liquor.

The primary sludge HTC liquor formed some solids, or slime, and changed color drastically between days. Figure 27 shows PS240 liquor over the course of two days. Primary sludge liquor was originally stored at room temperature and then in chilled water before moving it to a 4 ± 2°C refrigerator. This likely caused the change because the biosludge liquor placed directly in the refrigerator retained its color.

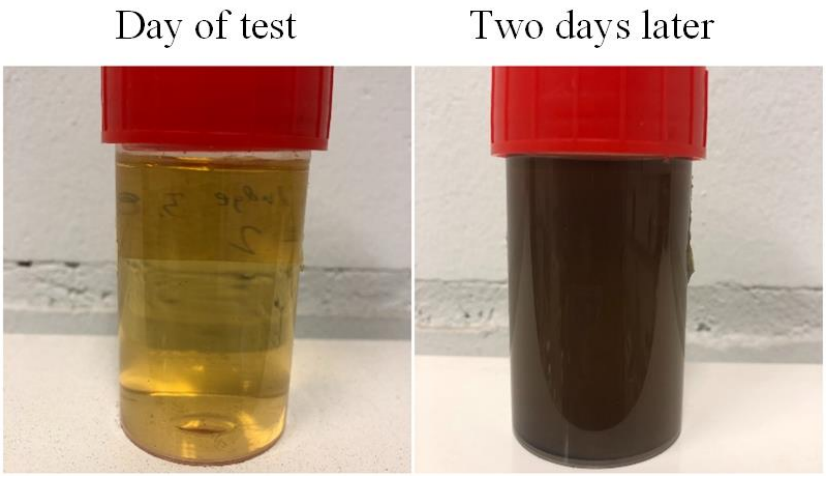

Figure 27. PS240 liquor color change.

The change in color of biosludge liquor did not seem to follow any trend. It was expected that the higher temperatures would have a darker color since part of the volatiles were dissolved into the liquor instead of remaining in the hydrochar, which also reduced its mass yield. Additionally, larger compounds tend to settle, so the diluted liquor was naturally collected in one vial and the more concentrated liquor in another, explaining the variance in color within the same trial. For this reason, sample was collected from both vials in the following tests.

Table 14 presents the liquid characterization for primary sludge and biosludge.

Table 14. Primary sludge and biosludge liquid fraction characterization.

		Primary sludge					**Biosludge**				
	°C	**Raw**	**180**	**200**	**220**	**240**	**Raw**	**180**	**200**	**220**	**240**
pH	--	7.67	5.19	4.79	4.35	4.08	8.65	7.17	6.31	7.40	6.93
NVR	g/kg	2.68	0.86	1.00	1.36	1.30	2.70	1.88	4.36	2.64	2.32
Inorganic		1.52	0.32	0.31	0.31	0.26	1.24	0.20	0.84	0.72	0.35
Organic		1.16	0.54	0.69	1.04	1.05	1.46	1.68	3.52	1.92	1.96
TC	g/L	4.08	3.10	2.66	3.38	3.11	6.98	5.21	13.42	8.76	11.46
TOC		4.04	3.07	2.63	3.35	3.08	4.34	4.67	12.97	8.20	11.42
IC		0.04	0.03	0.13	0.03	0.03	2.64	0.54	0.45	0.56	0.04
COD		4.90	2.40	4.30	6.70	8.10	7.70	12.60	34.50	25.30	33.10
COD/TOC	gO_2/gC	1.21	0.78	1.63	2.00	2.63	1.77	2.70	2.66	3.09	2.90

NVR: non-volatile residue; TC: total carbon; TOC: total organic carbon; IC: inorganic carbon; COD: chemical oxygen demand

pH

Generally, pH decreased after HTC at increasing reaction temperature for both primary sludge and biosludge. The alkaline nature of the raw sludge is due to the alkaline chemical conditions in the mill process and high content of green liquor dregs ($CaCO_3$) in the primary clarifier, in addition to further neutralization before secondary treatment (Pöykiö, Nurmesniemi, & Keiski, 2007). This explains why primary sludge started at a lower pH. Primary sludge also reduced more rapidly from 7.67 to 4.08 compared to biosludge, which reduced from 8.65 to 6.93 after undergoing HTC. The behavior of biosludge is also not as negatively linear as primary sludge since the pH oscillated between rising and falling as it decreased overall. HTC generates organic acids while it decomposes organic compounds, lowering the liquor pH (Mäkelä et al., 2018). Elemental sulfur, aluminum sulfate, and sulfuric acid are typically added to soil to lower the pH for plants that are intolerant of alkaline conditions (Combs, 2007). Using HTC liquor is a possible replacement for these additives, which can be dangerous and costly.

NVR, inorganic, and organic content

Like hydrochar, biosludge HTC liquor has a higher concentration of nutrients, in this case NVR, than primary sludge. Hoekman et al. (2013) noted that NVR decreased at a higher HTC reaction temperature due to non-volatile organic compounds continuing to react and break down into non-condensable gases. However, this was not entirely consistent for the present study except slightly decreasing from PS220 and more noticeably from BS200. Perhaps this is caused by primary sludge not being as affected by HTC, and biosludge starting to react at a higher temperature than the herbaceous and woody feedstocks tested in the aforementioned study. The percentage of inorganic content in the NVR decreased as the reaction temperature increased between raw filtrate and 240°C, from 57 to 20% in primary sludge and from 46 to 15% in biosludge, though biosludge experienced fluctuation between 180 and 220°C.

TC, TOC, IC, and COD

TOC and COD, displayed in Figure 28, are on average 2.57 and 4.29 times greater for biosludge than primary sludge, respectively. The larger data fall within the ranges presented earlier in Table 6 but the lower data fall beneath typical values, though pulp mill sludge is

not included. Primary sludge COD is between 2 and 9 g/L, biosludge between 7 and 35 g/L, and Mäkelä et al. (2018) chemical (tertiary) sludge between 16 and 47 g/L. This indicates that COD of sludge filtrate increases after each iteration of pulp mill wastewater treatment because the goal is to remove nutrients from the effluent before recycling or releasing to a water source. The COD/TOC ratios do not vary in a specific pattern but are generally greater for treated sludge liquor compared to raw sludge filtrate, suggesting an increase of oxidizable organic compounds due to HTC (Köchermann et al., 2018).

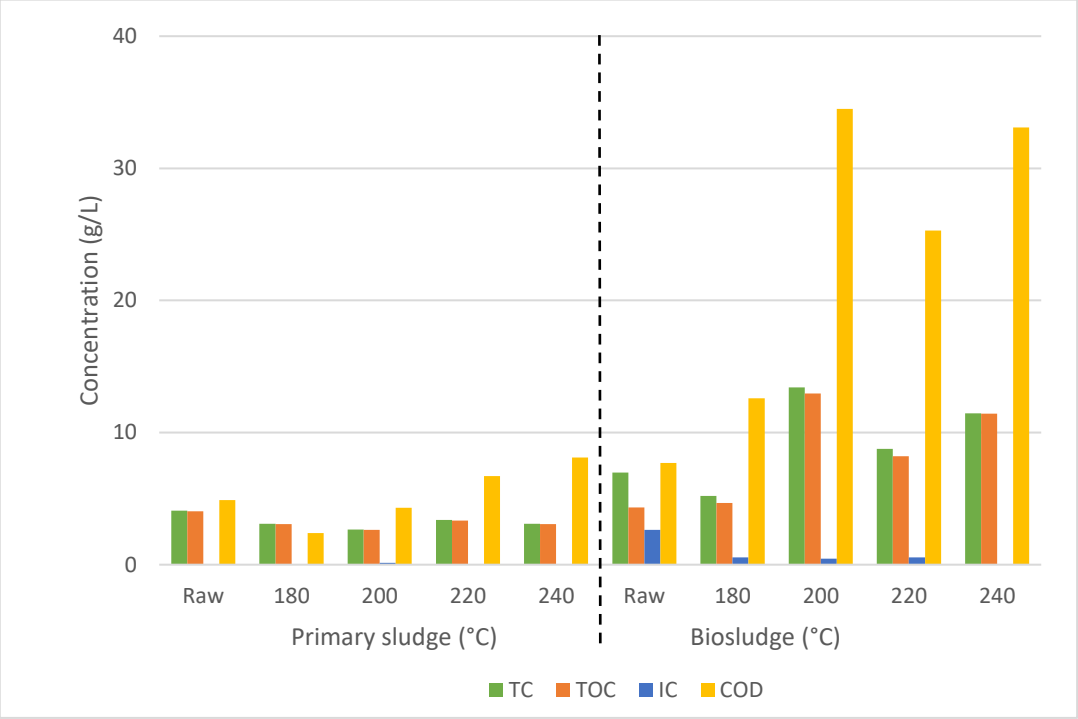

Figure 28. Carbon content and COD of primary sludge and biosludge.

Inductively coupled plasma optical emission spectrometry (ICP-OES)

The raw filtrate and HTC liquor contain a much higher trace elemental concentration than the solids. Figure 29 shows that the units of liquid and solid differed by a scale of 4 to 6. Overall, primary sludge HTC liquor is more concentrated than biosludge, with a total of 456 compared to 366 kg/kg, respectively, though the average is only about 20 kg/kg higher. This is due to the high accumulation of trace elements in dried biosludge and hydrochar, while they seem more likely to leach into the liquor for primary sludge. There was a slight correlation between solid and liquid accumulation. For example, K is the most concentrated element present in the HTC liquor at 61 kg/kg for BS180, which is the lowest, just 32 mg/kg,

in the hydrochar. This steep increase would suggest that K transferred from the hydrochar to the liquor due to HTC, which happens for some elements but appears to have no effect on others. Shi et al. (2013) showed that a higher HTC temperature leads to an increased heavy metal concentration, while Basso et al. (2015) did not find any trend based on process conditions, the latter of which is consistent with the present study.

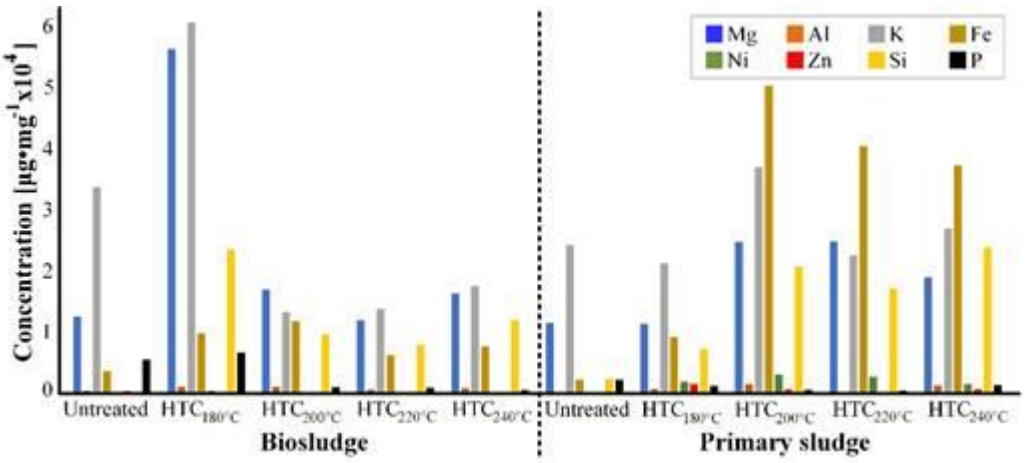

Figure 29. Trace elemental concentration of raw filtrate and HTC liquor.

7.2 HTC recirculation of biosludge

General analytical methods were performed for HTC recirculation. BS160_60 used biosludge from the first experimental condition and cannot be accurately compared to the remaining tests from the second batch of biosludge. Thus, BS160_60 data will appear in summary tables and pictures but not in graphs nor in all discussion.

7.2.1 Solid characterization

Since the recirculation experiments were performed on a smaller scale and there were low amounts of solid, only ash, volatiles, and FTIR were characterized for the hydrochar. One can notice from Figure 30 that hydrochar becomes increasingly powdery after multiple recirculations. This difference can especially be noted between BS160_40_3 and 4. Resultingly, the hydrochar also became easier to filter. Like in the first experimental condition, BS200 is lighter in color and consistently a powder compared to BS160. The recirculations at different dilutions look similar, though the appearance of BS160_40_4 transformed more than BS160_20_4.

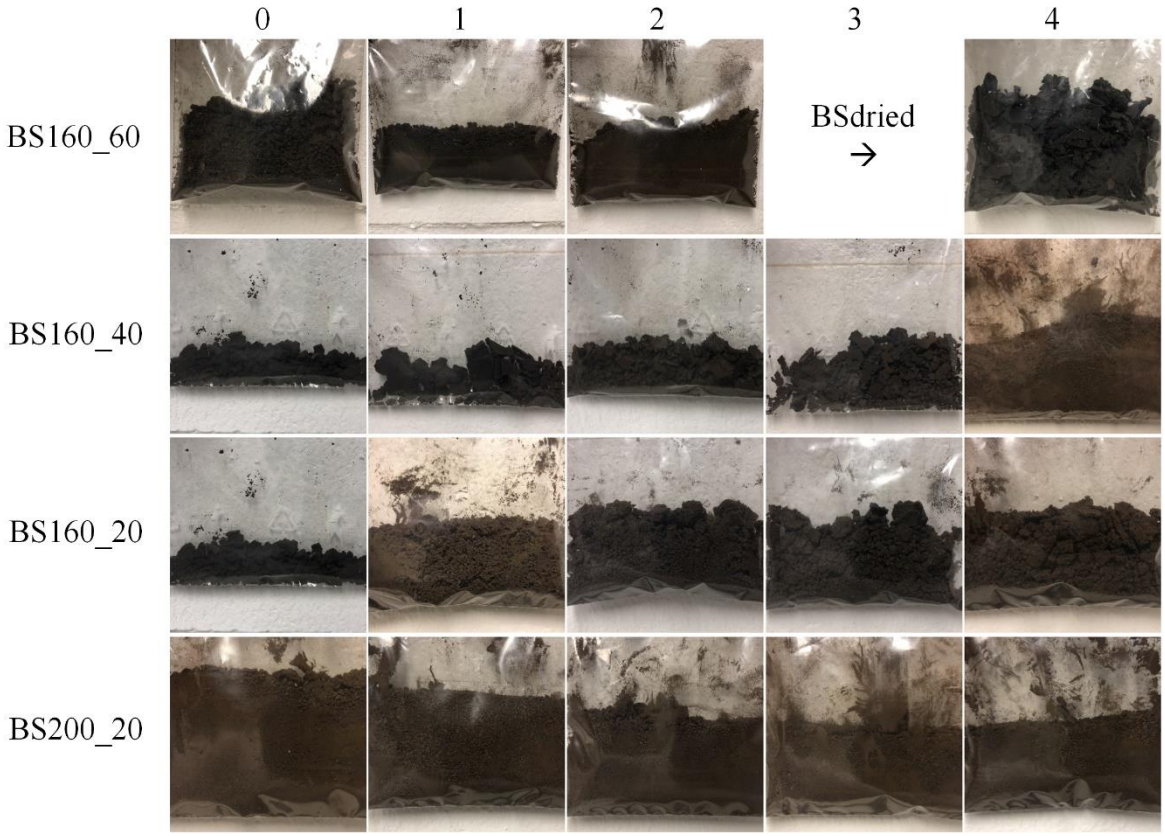

Figure 30. Dried biosludge and recirculated hydrochar.

Table 15 presents the main solid characteristics of the HTC recirculation.

Table 15. HTC recirculation solid characterization.

		Proximate analysis (% mass, dry)					**Heating value** (MJ/kg, dry)		
	Recirculation	**MY**	**MC**	**A**	**V**	**FC**	**HHV**	**ED** (--)	**EY** (%)
	BSdried	--	1.04	15.58	66.64	17.45	19.73	--	--
BS160_60	0	--	1.86	20.13	62.73	17.14	19.10	--	--
	1	--	3.00	19.41	61.65	18.93	19.89	--	--
	2	--	2.75	19.73	60.48	19.79	19.96	--	--
BS160_40	0	42.59	1.84	15.72	61.92	22.36	21.22	1.06	45.32
	1	80.17	1.38	15.59	61.03	23.39	21.37	1.07	85.95
	2	76.40	2.54	15.96	62.57	21.47	21.12	1.06	80.94
	3	79.80	1.66	15.71	62.49	21.79	21.06	1.06	84.29
	4	69.96	2.71	15.86	64.05	20.09	20.87	1.05	73.23
BS160_20*	1	77.52	2.75	16.26	63.50	20.24	20.82	1.04	80.97
	2	98.00	5.03	16.29	59.90	23.81	22.13	1.11	108.80
	3	95.03	3.84	16.26	59.77	23.97	21.90	1.10	104.41
	4	99.84	4.18	16.37	57.97	25.66	22.34	1.12	111.88
BS200_20	0	82.36	4.26	18.63	49.74	31.62	23.21	1.16	95.86
	1	82.53	4.60	18.98	52.17	28.86	22.58	1.13	93.47
	2	78.17	4.31	19.25	52.59	28.15	22.29	1.12	87.40
	3	78.54	4.00	19.12	52.53	28.35	22.29	1.12	87.82
	4	78.55	4.05	19.34	52.64	28.02	22.18	1.11	87.39

MY: mass yield; MC: moisture content; A: ash content; V: volatile matter; FC: fixed carbon; HHV: higher heating value, theoretical; ED: energy densification; EY: energy yield; *BS160_20_0 = BS160_40_0

Mass yield

The mass yield was expected to increase after each recirculation due to accumulation of solids from the HTC liquor. However, this was not the case. The values are inconsistent, ranging between 42 and 100%. The one consistency is that BS_1 has a higher mass yield than BS_0, but values variably increase and decrease thereafter. BS160_20 has the highest mass yield instead of BS160_40 in which more solids were introduced during each recirculation. Though most studies noticed an increase, Xu et al. (2020) found that mass yield of sewage sludge varied and generally decreased with additional recirculations.

Proximate analysis

Following their inverse proportionality, BS200_20 has the highest ash and lowest volatile matter content, while BS160_40 displays opposite behavior and BS160_20 is in the middle for both tests, shown in Figure 31. Subsequently, fixed carbon is proportional to ash content – highest for BS200_20 and lowest for BS160_40.

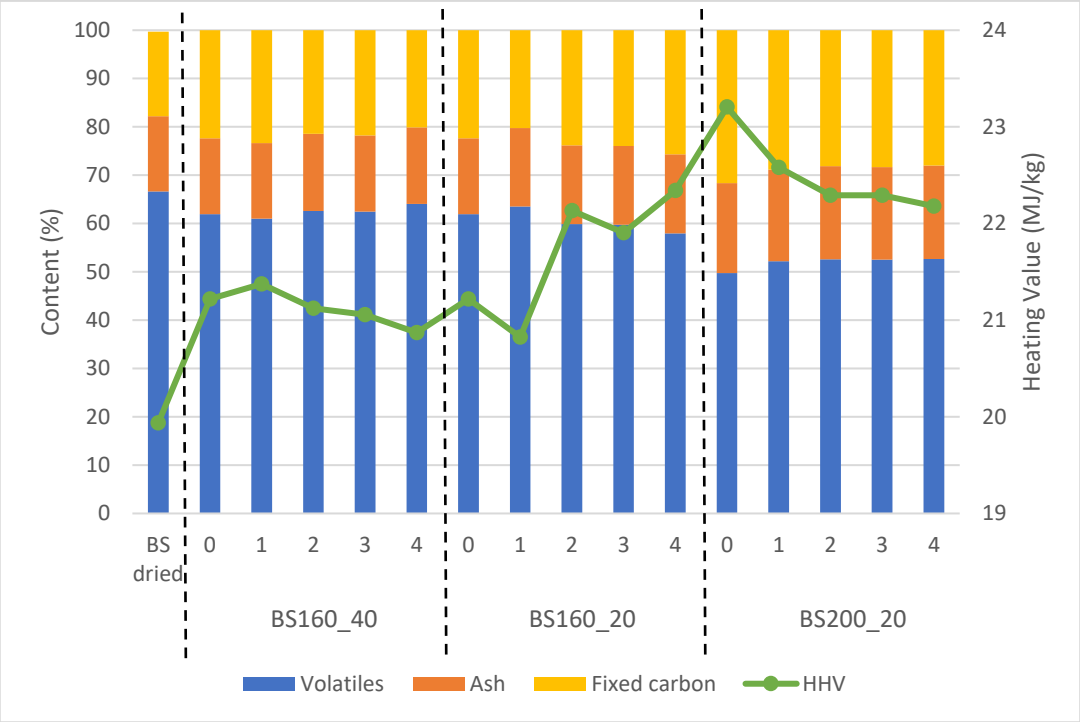

Figure 31. Proximate analysis and heating value of HTC recirculation.

Heating value

The $HHV_{dry,\ theoretical}$ equations were first applied to the biosludge hydrochar in the first experimental condition to compare for accuracy and choose the equation with the lowest error. $HHV_{dry,\ theoretical\_1}$, $HHV_{dry,\ theoretical\_2}$, and $HHV_{dry,\ theoretical\_3}$ on average have errors of 8.06, 12.35, and 16.13%, respectively. Thus, $HHV_{dry,\ theoretical\_1}$ was applied for HTC recirculation.

Like in the first experimental condition, all HTC treatments resulted in a higher HHV than BSdried. After that HHV generally decreased after each recirculation for BS160_40 and BS200_20 but increased for BS160_60 and BS160_20. BS160_60, BS160_40, BS160_20, and BS200_20 have an average HHV of 19.65, 21.13, 21.68, and 22.51 MJ/kg, respectively. This trend suggests that recirculating a higher percentage of liquor may inhibit HTC and confirms that a higher reaction temperature improves HTC.

Fourier-transform infrared spectroscopy (FTIR)

The recirculated hydrochar has the same peaks (kaolinite, O-H, and aromatic C=C) as biosludge in the first experimental condition. As seen in Figure 32, the hydrochar recirculated 4 times has the steepest peaks while BSdried has the shallowest peaks.

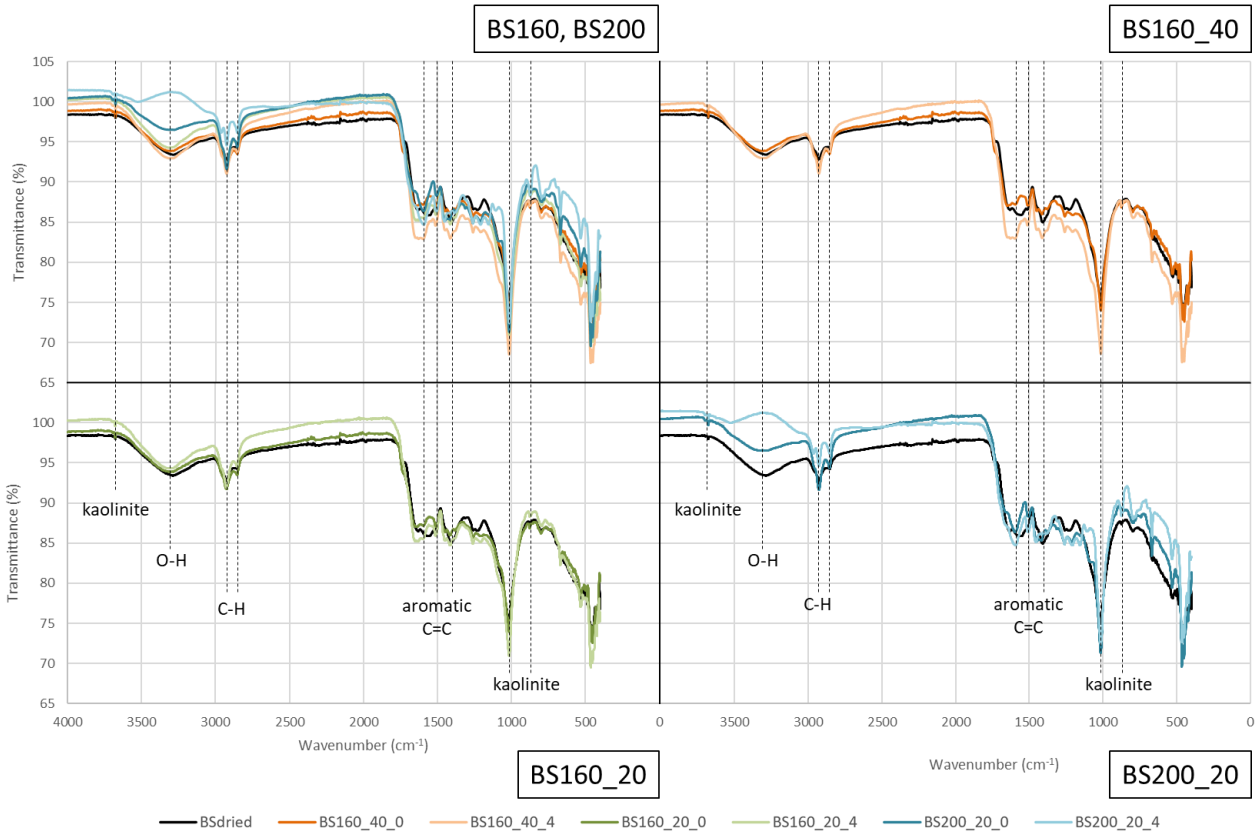

Figure 32. FTIR of recirculated biosludge hydrochar.

7.2.2 Liquid characterization

Figure 33 shows the recirculated HTC liquor. Raw biosludge filtrate is considerably lighter and more yellow than the treated liquor. BS160_60 appears the darkest of all trials due to its 20 to 40% higher dilution of HTC liquor. BS_0 is lighter for all runs except BS160_60, likely due to requiring the only overnight filtration in the recirculation experiments. Further recirculations appear similar but BS160_20 is lighter than BS160_40, which is also lighter than BS200_20. Overall, recirculation at a higher dilution darkens the shade of HTC liquor.

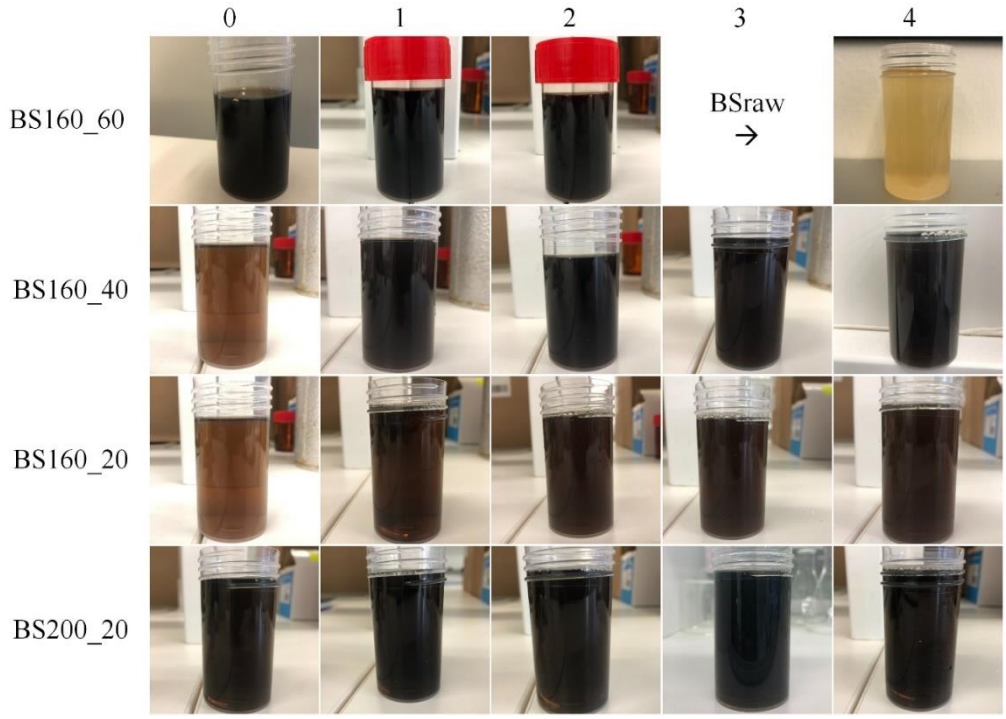

Figure 33. Biosludge filtrate and recirculated HTC liquor.

Table 16 summarizes the HTC liquor characteristics.

Table 16. HTC recirculation liquid characterization.

		pH	NVR	Inorganic	Organic
	Recirculation	--		g/kg	
	BSraw	7.83	2.28	1.39	0.88
BS160_60	0	7.24	13.05	2.15	10.89
	1	6.11	13.67	2.01	11.65
	2	5.64	20.03	2.85	17.18
BS160_40	0	6.33	4.17	0.84	3.33
	1	6.41	8.22	1.35	6.86
	2	5.71	9.14	1.67	7.47
	3	5.67	9.31	1.59	7.73
	4	5.67	6.89	1.22	5.68
BS160_20	1	5.75	6.80	1.02	5.78
	2	5.62	9.00	1.39	7.60
	3	5.61	8.87	1.27	7.60
	4	5.58	9.28	1.39	7.88
BS200_20	0	5.65	7.79	1.33	6.46
	1	5.65	8.82	1.59	7.23
	2	5.67	8.99	1.82	7.18
	3	5.87	8.83	1.70	7.13
	4	5.86	8.71	1.44	7.27

NVR: non-volatile residue; *BS160_20_0 = BS160_40_0

pH

pH tended to decrease after recirculation except for BS200_20, which incrementally increased. Different studies produced various results including a slight decrease in pH from 2.72 to 2.67 after recirculation until the 4th in which pH stabilized due to the reaction mechanism reaching equilibrium in Kambo, Minaret, & Dutta (2018). On the other hand, pH marginally increased from 5.41 to 6.02 and 4.8 to 5.3 caused by an accumulation of inorganic ions such as alkali and alkaline-earth metals (Zhang et al., 2020; Wang et al., 2019). Overall pH is not greatly affected by recirculation.

NVR, inorganic, and organic content

Similar to biosludge in the first experimental condition, the inorganic content reduced significantly after HTC, from 61% at BSraw to between 15 and 21% for the HTC liquor. NVR rose after BS_0 but fluctuated in subsequent recirculations. Otherwise, there is no significant pattern, which was the reason for not testing the trace elemental concentration of the HTC recirculation liquor. HTC liquor from the autoclaves produced an NVR content on a scale of about two times larger than in the first experimental condition. For example, BS200 has an NVR of 4.36 g/kg while it increased to 7.79 g/kg for BS200_20. This was caused by the smaller reactor size and amount of sample releasing fewer gases that were instead concentrated in the liquid.

8 LIMITATIONS AND FUTURE WORK

Though in this study each procedure was carried out as precisely as possible, some sources of inaccuracy arose due to human error and other constraints. For example, it was particularly difficult to consistently obtain an accurate solid measurement. The biosludge sample in the second experimental condition had a higher moisture content and was a homogenous mixture, unlike the first sample, in which the solids had already settled. Later this was discovered to be due to thawing. This caused filtering to vary between samples that were used fresh or after being frozen. Often some of the sample was lost on the filter. Once the reactor heated too quickly, which resulted in a rise in pressure and slurry leaking from the reactor tube. Additional error emerged in the XRD crystallinity calculations since the data has a lot of background noise, making it difficult to identify peaks. The biosludge liquor in the first experimental condition varied widely in color. Since the biosludge did not filter easily, deionized water was used to wash out the collection container in attempt to retrieve as much solid as possible. The amount of water used may have differed between trials, altering the color of the liquor. Additionally, better camera conditions could have improved qualitative analysis of the liquor color.

Furthermore, mass yield of the recirculation varied in unexpected ways. This could be due to variance in filtering the biosludge before HTC and the liquor after, leaking in the autoclaves, the small sample size, and the number of recirculations not providing enough data. Additionally, testing the trace elemental concentration, COD, and TOC could provide interesting results and explain some of the recirculation behavior. In the future it is recommended to recirculate HTC liquor in the 1 L reactor in order to test a larger sample and higher temperatures, which are predicted to affect the reaction. It would also be worthwhile to analyze the HTC liquor for its biogas potential both before and after recirculation.

9 CONCLUSION

In this study, two experimental conditions were tested to characterize HTC of primary sludge and biosludge as well as the recirculation of biosludge HTC liquor. Biosludge and its filtrate were generally found to have a higher ash, carbon, nutritional, and trace elemental content than primary sludge, and the impact of HTC was more significant. HTC at higher temperatures increased the HHV of primary sludge and biosludge, and biosludge was transformed to a material similar to the lower energy density coal, lignite. Therefore, biosludge would be a suitable option for energy applications. While hydrochar is an attractive option for soil amendment as well, some of the metal limits are exceeded for soils in the untreated as well as treated solid sludge. The liquid fraction contains metals at a level about five times higher than solids. HTC liquor could be beneficial for decreasing soil pH, but metals would need to be reduced before soil amendment could be considered.

Furthermore, recirculation did not have as large of an effect as expected and the data varied widely. The proximate analysis is similar to that of the first experimental condition, and the calculated HHV was affected more by temperature than by number of recirculations, One interesting finding was that the HHV generally increased as the dilution decreased, indicating that accumulation of solids could have adverse effects on the heating value. pH changed only minimally, and NVR increased after BS_0 but not considerably after that. Overall, recirculation did not have a significant impact on biosludge, suggesting that HTC liquor could be recycled for the purpose of saving water but not for the intent of improving properties for energy and soil amendment applications. Overall, HTC is a promising treatment for pulp mill sludge, and its prospects can be promoted by further research.

REFERENCES

Ameen, M. et al. 2021. Effect of acid catalysts on hydrothermal carbonization of Malaysian oil palm residues (leaves, fronds, and shells) for hydrochar production. *Biomass Conversion and Biorefinery*, 12 p.

Amutio, M. et al. 2012. Kinetic study of lignocellulosic biomass oxidative pyrolysis. *Fuel*, **95**, p. 305-311.

Baccile, N. et al. 2013. Characterization of Hydrothermal Carbonization Materials. In: *Sustainable Carbon Materials from Hydrothermal Processes.* Chichester: Wiley, p. 151-211. ISBN 978-1-11997-539-7.

Bargmann, I. et al. 2014. Effects of hydrochar application on the dynamics of soluble nitrogen in soils and on plant availability. *Journal of Plant Nutrition and Soil Science*, **177**, p. 48-58.

Basso, D. et al. 2015. Hydrothermal carbonization of off-specification compost: A byproduct of the organic municipal solid waste treatment. *Bioresource Technology*, **182**, p. 217-224.

Basu, P. 2013. *Biomass Gasification, Pyrolysis and Torrefaction : Practical Design and Theory.* Second edition. Amsterdam: Academic Press, p. 147-176; 199-248. ISBN 9780123964885.

Batidzirai, B.; Smeets, E.; Faaij, A. 2012. Harmonising bioenergy resource potentials—Methodological lessons from review of state of the art bioenergy potential assessments. *Renewable and Sustainable Energy Reviews*, **16**(9), p. 6598-6630.

Bergman, P.; Kiel, J. 2005. Torrefaction for biomass upgrading. Paris: 14th European Biomass Conference & Exhibition, 8p.

Bhatt, D. et al. 2018. Hydrothermal Carbonization of Biosolids from Waste Water Treatment Plant. *Energies*, **11**(9), p. 2286.

Bonilla, S.; Tran, H.; Allen, D. 2015. Enhancing pulp and paper mill biosludge dewaterability using enzymes. *Water Research*, **68**, p. 692-700.

Cabrera, M. 2017. Pulp Mill Wastewater: Characteristics and Treatment. *Biological Wastewater Treatment and Resource Recovery*, p. 119-136.

C-Green. [Accessed 25 May 2021]. Available from https://www.c-green.se/

Chong, K.; Chia, C.; Zakaria, S. 2014. Polymorphs calcium carbonate on temperature reaction. *AIP Conference Proceedings*, **1614**, p. 52-56.

Chum, H.; Faaij, A.; Moreira, J. 2011. Bioenergy. In: *IPCC Special Report on Renewable Energy Sources and Climate Change Mitigation*. Cambridge: Cambridge University Press, p. 209-332. Available from https://www.ipcc.ch/site/assets/uploads/2018/03/Chapter-2-Bioenergy-1.pdf

Collivignarelli, M. et al. 2019. Legislation for the Reuse of Biosolids on Agricultural Land in Europe: Overview. *Sustainability*, **11**(21), p. 6015-6036.

Combs, S. 2007. Reducing Soil pH. *Wisconsin Horticulture.* [Accessed 28 May 2021]. Available from https://hort.extension.wisc.edu/articles/reducing-soil-ph/

Cremers, M. et al. 2015. Status overview of torrefaction technologies. IEA Bioenergy. ISBN: 978-1-910154-23-6. Available from https://www.ieabioenergy.com/wp-content/uploads/2015/11/IEA_Bioenergy_T32_Torrefaction_update_2015b.pdf

Demirbas, A. 2004. Combustion characteristics of different biomass fuels. *Progress in Energy and Combustion Science*, **30**(2), p. 219-230.

Dornburg, V. et al. 2010. Bioenergy revisited: Key factors in global potentials of bioenergy. *Energy & Environmental Science*, **3**, p. 258-267.

Elbersen, B. et al. 2012. Atlas of EU biomass potentials. Deliverable 3.3: Spatially detailed and quantified overview of EU biomass potential taking into account the main criteria determining biomass availability from different sources. *Biomass Futures,* 139 p. IEE 08 653 SI2. 529 241. Available from https://ec.europa.eu/energy/intelligent/projects/sites/iee-projects/files/projects/documents/biomass_futures_atlas_of_technical_and_economic_biomass_potential_en.pdf

Eskandari, S. et al. 2019. Hydrochar-Amended Substrates for Production of Containerized Pine Tree Seedlings under Different Fertilization Regimes. *Agronomy*, **9**(7), p.350-366.

European Commission [a]. Glossary: Carbon dioxide equivalent. [Accessed 26 May 2021]. Available from https://ec.europa.eu/eurostat/statistics-explained/index.php?title=Glossary:Carbon_dioxide_equivalent

European Commission [b]. Paris Agreement. [Accessed 11 January 2021]. Available from https://ec.europa.eu/clima/policies/international/negotiations/paris_en

European Commission. Sewage sludge production and disposal. [Accessed 1 December 2020]. Available from https://ec.europa.eu/eurostat/web/products-datasets/product?code=env_ww_spd

European Parliament. Circular economy: definition, importance and benefits. [Accessed 28 May 2021]. Available from https://www.europarl.europa.eu/news/en/headlines/economy/20151201STO05603/circular-economy-definition-importance-and-benefits

The European Parliament and the Council of the European Union. 2019. Regulation (EU) 2019/1009 laying down rules on the making available on the market of EU fertilizing products. *Official Journal of the European Union*, **62**, 114 p.

FAO. Global production and trade in forest products in 2018. [Accessed 8 December 2020]. Available from http://www.fao.org/forestry/statistics/80938/en/

Faubert, P. et al. 2016. Pulp and paper mill sludge management practices: What are the challenges to assess the impacts on greenhouse gas emissions? *Resources, Conservation and Recycling*, **108**, p. 107-133.

Ferrentino, R. et al. 2020. Coupling Hydrothermal Carbonization with Anaerobic Digestion for Sewage Sludge Treatment: Influence of HTC Liquor and Hydrochar on Biomethane Production. *Energies*, **13**(23), p. 6262.

Gaines, L. 2004. Recycling of Paper. *Encyclopedia of Energy*, **5**, p. 253-260.

Gavrilescu, D. 2013. Pulping Fundamentals and Processing. In: Valentin, P., *Pulp Production and Processing: From Papermaking to High-tech Products*. Shrewsbury: Smithers Rapra Technology Ltd, p. 35-70. ISBN 978-1-84735-637-6.

Ghetti, P.; Ricca, L.; Angelini, L. 1996. Thermal analysis of biomass and corresponding pyrolysis products. *Fuel*, **75**(5), p. 565-573.

Heidari, M. et al. 2019. A review of the current knowledge and challenges of hydrothermal carbonization for biomass conversion. *Journal of the Energy Institute*, **92**(6), p. 1779-1799.

Hoekman, S. et al. 2013. Hydrothermal carbonization (HTC) of selected woody and herbaceous biomass feedstocks. *Biomass Conversion and Biorefinery*, **3**, p. 113-126.

HTCycle. [Accessed 25 May 2021]. Available from https://htcycle.ag/en

Huang, H.; Yuan, X. 2016. The migration and transformation behaviors of heavy metals during the hydrothermal treatment of sewage sludge. *Bioresource Technology*, **200**, p. 991-998.

Huang, Z. et al. 2021. Effect of ionic liquid assisted hydrothermal carbonization on the properties and gasification reactivity of hydrochar derived from eucalyptus. *Journal of Colloid and Interface Science*, **586**, p. 423-432.

Ingelia. [Accessed 25 May 2021]. Available from https://ingelia.com/?lang=en

IPCC. 2018. Global Warming of 1.5°C, 630 p. Available from https://www.ipcc.ch/sr15/

Kambo, H.; Minaret, J.; Dutta, A. 2018. Process Water from the Hydrothermal Carbonization of Biomass: A Waste or a Valuable Product? *Waste and Biomass Valorization,* **9**, p. 1181-1189.

Kang, S. et al. 2012. Characterization of Hydrochars Produced by Hydrothermal Carbonization of Lignin, Cellulose, D-Xylose, and Wood Meal. *Industrial & Engineering Chemistry Research,* **51**, p. 9023-9031.

Karaca, C; Erdoğdu, M. 2013. Sustainable Development and Turkey's Biomass Energy Potential. In: *Economic Behavior, Game Theory, and Technology in Emerging Markets.* Hershey: IGI Global, p. 335-358. ISBN 978-1-46664-745-9.

Karp, A.; Halford, N. 2011. Energy Crops: Introduction. In: *Energy Crops*. Cambridge: Royal Society of Chemistry, 12 p. ISBN 978-1-84973-032-7.

Kelessidis, A.; Stasinakis, A. 2012. Comparative study of the methods used for treatment and final disposal of sewage sludge in European countries. *Waste Management*, **32**(6), p. 1186-1195.

Khoshbouy, R. et al. 2018. Effect of acid-assisted hydrothermal carbonization (HTC) process of tree branches using nitric acid on cadmium adsorption. *E3S Web of Conferences*, **67**, p. 03033.

Kieseler, S.; Neubauer, Y.; Zobel, N. 2013. Ultimate and Proximate Correlations for Estimating the Higher Heating Value of Hydrothermal Solids. *Energy Fuels,* **27**(2), p. 908-918.

Kogbara, R. et al. 2020. Dataset on the influence of gas-to-liquid biosludge on arid soil properties and growth performance of alfalfa. *Data in Brief,* **28**, p. 105074.

Kuparinen, K. et al. 2019. Biosludge utilization in the forest industry- trends and effect to modern mills. Lappeenranta: School of Energy Systems, Lappeenranta-Lahti University of Technology LUT, 77 p.

Köchermann, J. et al. 2018. Hydrothermal carbonization: Temperature influence on hydrochar and aqueous phase composition during process water recirculation. *Journal of Environmental Chemical Engineering*, **6**(4), p. 5481-5487.

Langone, M.; Basso, D. 2020. Process Waters from Hydrothermal Carbonization of Sludge: Characteristics and Possible Valorization Pathways. *International Journal of Environmental Research and Public Health*, **17**(18), p. 6618.

Lindsey, R. 2020. Climate Change: Atmospheric Carbon Dioxide. [Accessed 7 January 2021]. Available from https://www.climate.gov/news-features/understanding-climate/climate-change-atmospheric-carbon-dioxide

Lohiniva, E.; Mäkinen, T.; Sipilä, K. 2001. Sludge treatment new and presently employed technologies. VTT Research Notes 2081. Espoo: VTT Technical Research Center of Finland, p. 3-146.

Ma, Z. et al. 2018. Comparison of the thermal degradation behaviors and kinetics of palm oil waste under nitrogen and air atmosphere in TGA-FTIR with a complementary use of model-free and model-fitting approaches. *Journal of Analytical and Applied Pyrolysis*, **134**, p. 12-24.

Méndez, A. et al. 2009. Characterization and pyrolysis behaviour of different paper mill waste materials. *Journal of Analytical and Applied Pyrolysis*, **86**, p. 66-73.

Mendoza Martinez et al. 2021. Hydrothermal carbonization of lignocellulosic agro-forest based biomass residues. *Biomass and Bioenergy*, **147**, p. 106004.

Meyer, T. et al. 2018. Dewatering of pulp and paper mill biosludge and primary sludge. Toronto: Department of Chemical Engineering and Applied Chemistry, University of Toronto, 23 p.

Mohammadi, A. et al. 2019. Environmental analysis of producing biochar and energy recovery from pulp and paper mill biosludge. *Journal of Industrial Ecology*, **23**, p. 1039-1051.

Molino, A.; Chianese, S.; Musmarra, D. 2016. Biomass gasification technology: The state of the art overview. *Journal of Energy Chemistry*, **25**(1), p. 10-25.

Mowla, D.; Tran, H.; Allen, D. 2013. A review of the properties of biosludge and its relevance to enhanced dewatering processes. *Biomass and Bioenergy*, **58**, p. 365-378.

Mäkelä, M.; Benavente, V.; Fullana, A. 2015. Hydrothermal carbonization of lignocellulosic biomass: Effect of process conditions on hydrochar properties. *Applied Energy*, **155**, p. 576-584.

Mäkelä, M. et al. 2018. Process water properties from hydrothermal carbonization of chemical sludge from a pulp and board mill. *Bioresource Technology*, **263**, p. 654-659.

Nhuchhen, D.; Salam, P. 2012. Estimation of higher heating value of biomass from proximate analysis: A new approach. *Fuel*, **99**, p. 55-63.

Niinipuu, M. et al. 2020. The impact of hydrothermal carbonization on the surface functionalities of wet waste materials for water treatment applications. *Environmental Science and Pollution Research*, **27**, p. 24369-24379.

Pritchard, D. et al. 2010. Land application of sewage sludge (biosolids) in Australia: risks to the environment and food crops. *Water Science & Technology*, **62**(1), p. 48-57.

Pöykiö, R. et al. 2014. Chemical characterisation of biosludge from a wastewater treatment plant in a neutral sulphite semi-chemical pulp mill by single and sequential extraction of heavy metals and micro-/macronutrients– a case study. *Chemical Papers*, **68**(11), p. 1546-1554.

Pöykiö, R.; Nurmesniemi, H.; Keiski, R. 2007. Environmental risk assessment of heavy metal extractability in a biosludge from the biological wastewater treatment plant of a pulp and paper mill. *Environmental Monitoring and Assessment*, **128**, p. 153-164.

Pöykiö, R; Watkins, G.; Dahl, O. 2018. Characterization of primary and secondary wastewater treatment sludge from a pulp and board mill complex to evaluate the feasibility of utilization as a soil amendment agent and a fertilizer product. *Journal of Bioresources and Bioproducts*, **3**(3), p. 88-95.

REN21. 2017. Renewables 2017 Global Status Report. 302 p. ISBN 978-3-9818107-6-9. Available from https://www.ren21.net/wp-content/uploads/2019/05/GSR2017_Full-Report_English.pdf

Reza, M. 2015. Hydrothermal Carbonization (HTC) of Wheat Straw: Influence of Feedwater pH Prepared by Acetic acid and Potassium hydroxide. *Bioresource Technology*, **182**, p. 336-344.

Ritchie, H.; Roser, M. 2020. Energy. [Accessed 6 January 2021]. Available from https://ourworldindata.org/energy

Rodrigues, B. et al. 2021. Wet route pellets production using primary sludge from kraft pulp mill. *Nordic Pulp & Paper Research Journal*, 10 p.

Saha, N. et al. 2019. Hydrothermal Carbonization of Various Paper Mill Sludges: An Observation of Solid Fuel Properties. *Energies*, **12**(5), p. 858-875.

Salimi, M. et al. 2017. Optimizing the Preparation of Meso- and Microporous Canola Stalk Derived Hydrothermal Carbon via Response Surface Methodology for Methylene Blue Removal. *Energy Fuels*, **31**, p. 12327-12338.

Scott, G.; Smith, A.; Abubakr, S. 1995. Sludge Characteristics and Disposal Alternatives for the Pulp and Paper Industry. *Proceedings of the 1995 International Environmental Conference*, p. 269-279.

Shi, W. et al. 2013. Immobilization of heavy metals in sewage sludge by using subcritical water technology. *Bioresource Technology*, **137**, p. 18-24.

Shortall, O. 2013. "Marginal land" for energy crops: Exploring definitions and embedded assumptions. *Energy Policy*, **62**, p. 19-27.

Smeets, E. et al. 2007. A bottom-up assessment and review of global bio-energy potentials to 2050. *Progress in Energy and Combustion Science*, **33**(1), p. 56-106.

Stemann, J.; Putschew, A.; Ziegler, F. 2013. Hydrothermal carbonization: process water characterization and effects of water recirculation. *Bioresource Technology*, **143**, p. 139-146.

Stemann, J.; Ziegler, F. 2011. Assessment of the energetic efficiency of a continuously operating plant for hydrothermal carbonisation of biomass. *Proceedings of World Renewable Energy Congress 2011 – Sweden*, p. 125-132.

SunCoal. [Accessed 27 May 2021]. Available from https://www.suncoal.com

Tasca, A. et al. 2019. Hydrothermal carbonization of sewage sludge: A critical analysis of process severity, hydrochar properties and environmental implications. *Waste Management*, **93**, p. 1-13.

Techinstro. Hydrothermal Autoclave Reactor. [Accessed 17 February 2021]. Available from https://www.techinstro.com/hydrothermal-autoclave-reactor/

TerraNova Energy. [Accessed 25 May 2021]. Available from https://terranova-energy.com/en/

Thipkhunthod, P. et al. 2005. Predicting the heating value of sewage sludges in Thailand from proximate and ultimate analyses. *Fuel*, **84**(7-8), p. 849-857.

Trilokesh, C.; Uppuluri, K. 2019. Isolation and characterization of cellulose nanocrystals from jackfruit peel. *Scientific Reports*, **9**, p. 16709.

Tsai, W. et al. 2009. Production of pyrolytic liquids from industrial sewage sludges in an induction-heating reactor. *Bioresource Technology*, **100**(1), p. 406-412.

United Nations Environment Programme. 2020. *Emissions Gap Report 2020*. Nairobi. 128 p. ISBN 978-92-807-3812-4.

Usman, M. et al. 2019. Characterization and utilization of aqueous products from hydrothermal conversion of biomass for bio-oil and hydro-char production: a review. *Green Chemistry*, **21**, p. 1553-1572.

Van Loo, S.; Koppejan, J. 2008. *The handbook of biomass combustion and co-firing.* London: Earthscan, 442 p. ISBN 978-1-84407-249-1.

Vesilind, P.; Martel, C. 1989. Freezing of water and wastewater sludges. *Journal of Environmental Enigineering*, **116**, p. 854-861.

Wainaina, S. et al. 2019. Bioengineering of anaerobic digestion for volatile fatty acids, hydrogen or methane production: A critical review. *Bioengineered*, **10**(1), p. 437-458.

Wang, D. et al. 2018. Can hydrothermal pretreatment improve anaerobic digestion for biogas from lignocellulosic biomass? *Bioresource Technology*, **249**, p. 117-124.

Wang, F. et al. 2019. Effects of process water recirculation on solid and liquid products from hydrothermal carbonization of *Laminaria*. *Biosource Technology*, **292**, p. 121996.

Wang, M. et al. 2012. Well-to-wheels energy use and greenhouse gas emissions of ethanol from corn, sugarcane and cellulosic biomass for US use. *Environmental Research Letters*, **7**(4), 13 p.

Wang, Q.; Chen, W.; Jang, M. 2020. Characterization of Hydrochar Produced by Hydrothermal Carbonization of Organic Sludge. *Future Cities and Environment*, **6**(1), 10 p.

World Bioenergy Association. 2020. WBA Global Bioenergy Statistics 2020, 64 p. Available from https://worldbioenergy.org/uploads/201210%20WBA%20GBS%202020.pdf

Xu, J. 2020. Effect of spent liquor recycle during hydrothermal carbonization on the properties of hydrochar. *Water Science Technology*, **82**(12), p. 3017-3022.

Xu, Z. et al. 2020. Hydrothermal carbonization of sewage sludge: Effect of aqueous phase recycling. *Chemical Engineering Journal*, **387**, p. 123410.

Yang, G.; Zhang, G.; Wang, H. 2015. Current state of sludge production, management, treatment and disposal in China. *Water Research*, **78**, p. 60-73.

Zhang, C. et al. 2015. Effect of Residence Time on Hydrothermal Carbonization of Corn Cob Residual. *BioResources*, **10**(3), p. 3979-3986.

Zhang, C. et al. 2020. Co-hydrothermal Carbonization of Water Hyacinth and Sewage Sludge: Effects of Aqueous Phase Recirculation on the Characteristics of Hydrochar. *Energy Fuels*, **34**(11), p. 14147–14158.

Zheng, G.; Koziński, J. 2000. Thermal events occurring during the combustion of biomass residue. *Fuel*, **79**(2), p. 181-192.

APPENDICES

Appendix 1. Biosludge properties

Table 17. Biosludge properties from 5 pulp and paper mills (Kuparinen et al., 2019).

	Mill	A	B	C	D	E	Average
Dry solids content	%	9	3	12	0.97	2.4	5.5
Ash (575 ^{0}C)		16	24	13	38	29	24.0
Ash (815 ^{0}C)		15	24	--	37	25	25.3
C	% ds	44.2	38.6	46.2	31.9	37.2	39.6
H		6	5.1	6.4	3.8	5	5.3
N		6.7	3.4	5.3	3.6	4.2	4.6
Na	g/kgds	7300	20000	5800	60100	37000	26040
K		2800	2900	1700	5000	1500	2780
S		12200	25000	17600	37000	16000	21560
Ca		17000	26000	17000	21000	41000	24400
Si		21000	17000	9900	36000	23000	21380
Cl		3500	4400	3500	3500	51000	13180
Al		3300	23000	3700	17000	6300	10660
Fe		3200	6900	3000	23000	3500	7920
Mg		11000	6300	2100	7100	10000	7300
P		7900	5400	4600	5900	5600	5880
Mn	mg/kgds	6400	8300	1070	2100	7000	4974
Zn		300	920	630	95	710	531.0
Ba		550	460	--	200	300	378
Ti		120	180	--	440	170	228
V		< 10	67	--	35	34	45.3
Cr		60	45	29	29	57	44.0
Ni		53	48	13	19	70	40.6
Cu		36	38	37	42	26	35.8
F		52	32	0	58	< 25	35.5
Pb		7.9	40	13	7.4	15	16.7
Co		< 4	16	21	< 4	10	15.7
Cd		8	5	6	0.7	8.6	5.7
As		5.6	3	--	4.6	2.2	3.9
Sb		< 0.5	0.5	--	< 0,5	< 0,5	0.5
Hg		< 0.1	< 0.1	0.6	< 0.1	0.1	0.4
Tl		0.45	0.08	--	0.26	0.32	0.3
Se		< 0.2	< 0.2	--	< 0.2	< 0.2	< 0.2
HHV, dry solids	MJ/kgds	19.03	16.1	--	13.88	15.6	16.2
LHV, dry solids		17.34	14.2	--	11.88	14	14.4

Appendix 2. Fourier-transform infrared spectroscopy (FTIR)

Table 18. Primary sludge and biosludge FTIR peaks.

Primary sludge						
°C	Dried		180		240	
Peak	Wavelength (cm^{-1})	Transmittance (%)	Wavelength (cm^{-1})	Transmittance (%)	Wavelength (cm^{-1})	Transmittance (%)
1	3332	90.99	3336	87.97	3336	87.01
2	2895	94.65	2899	93.03	2900	92.31
3	1716	97.16	1716	96.37	1708	95.01
4	1603	97.47	1605	96.91	1602	95.91
5	1428	94.49	1428	92.69	1429	91.30
6	1315	91.99	1316	89.28	1315	87.36
s	1203	95.17	1203	92.97	1203	90.78
8	1161	88.55	1161	85.32	1160	82.13
9	1105	82.73	1105	78.17	1105	74.43
10	1028	70.41	1029	63.94	1030	57.78
11	897	87.55	897	85.47	899	85.51
Biosludge						
°C	Dried		180		240	
Peak	Wavelength (cm^{-1})	Transmittance (%)	Wavelength (cm^{-1})	Transmittance (%)	Wavelength (cm^{-1})	Transmittance (%)
1	3677	100.70	3677	98.19	3677	98.04
2	3279	98.25	3334	97.78	3299	94.65
3	2928	98.30	2922	93.80	2925	94.40
4	2866	98.83	2852	95.40	2854	95.58
5	1634	96.35	1591	91.91	1632	90.09
6	1515	96.5	1504	93.34	1513	90.68
7	1409	96.31	1451	90.74	1415	90.59
8	1228	96.47	1209	91.73	1224	91.03
9	1014	93.68	1017	80.12	1014	81.37
10	865	96.42	866	92.87	867	90.87

Appendix 3. Scanning electron microscopy (SEM) mapping

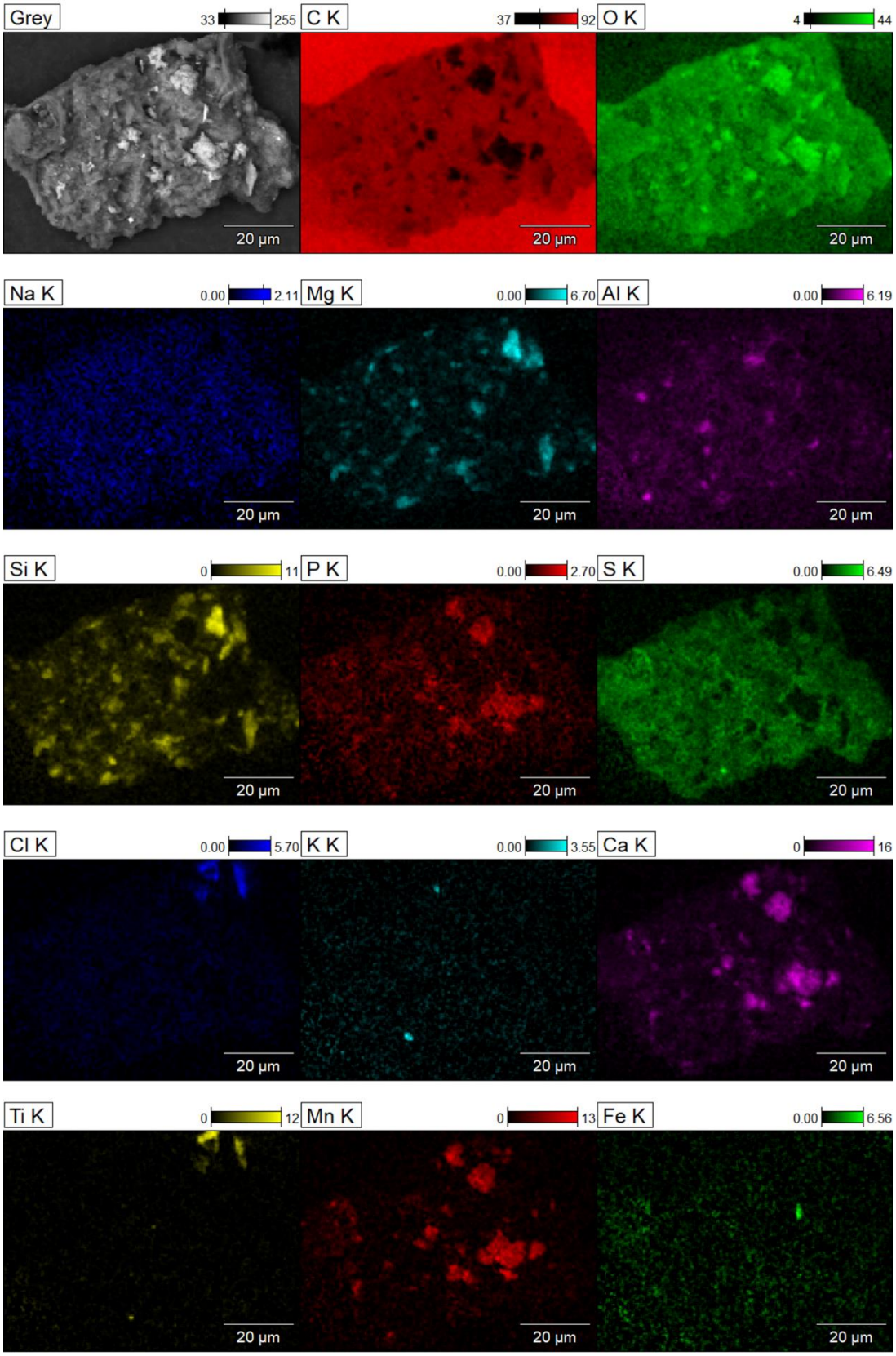

Figure 34. SEM mapping of BSdried.